



OPEN ACCESS

EDITED BY

Mehrab Momennia,
Michoacana University of San Nicolás
de Hidalgo, Mexico

REVIEWED BY

Izzet Sakalli,
Eastern Mediterranean
University, Türkiye
Shreyas Punacha,
University of Washington, United States

*CORRESPONDENCE

Seyed Naseh Sajadi,
✉ naseh.sajadi@gmail.com

RECEIVED 26 November 2025

REVISED 18 January 2026

ACCEPTED 30 January 2026

PUBLISHED 26 March 2026

CITATION

Ponglertsakul S and Sajadi SN (2026)
Analytic approximate charged black
hole solutions in Einstein–quartic
gravity.
Front. Astron. Space Sci. 13:1754814.
doi: 10.3389/fspas.2026.1754814

COPYRIGHT

© 2026 Ponglertsakul and Sajadi. This is
an open-access article distributed
under the terms of the [Creative
Commons Attribution License \(CC BY\)](#).
The use, distribution or reproduction in
other forums is permitted, provided the
original author(s) and the copyright
owner(s) are credited and that the
original publication in this journal is
cited, in accordance with accepted
academic practice. No use, distribution
or reproduction is permitted which
does not comply with these terms.

Analytic approximate charged black hole solutions in Einstein–quartic gravity

Supakchai Ponglertsakul and Seyed Naseh Sajadi*

Strong Gravity Group, Department of Physics, Faculty of Science, Silpakorn University, Nakhon
Pathom, Thailand

In this work, we employ continued fraction expansions to derive analytical, approximate charged black hole solutions in Einstein–Maxwell–quartic gravity, a theory that introduces quartic curvature corrections to the Einstein–Hilbert action. To construct the full solution, we first obtain the metric function near the event horizon and at asymptotically large distances and then smoothly connect these regions using the continued fraction method. We further compute the associated thermodynamic quantities and verify the validity of the first law of black hole thermodynamics and the Smarr relation within this framework. We find that the thermodynamic analysis reveals van der Waals-type phase transitions between small and large black holes, with critical parameters that exhibit a universal ratio independent of the model parameters. Furthermore, the quasi-normal mode analysis indicates that the resulting spacetime is dynamically stable.

KEYWORDS

charged black hole, continued fraction expansion, Einstein–quartic gravity, quasi-normal mode, thermodynamics of black hole

1 Introduction

To understand the physics of the universe across different scales, higher-curvature gravity theories have garnered significant attention. These theories extend Einstein’s general relativity by incorporating higher-order curvature terms in the action. Such corrections naturally arise from the renormalization of quantum field theories in curved spacetime and in the construction of low-energy effective actions of string theory. One key motivation for studying classical higher-curvature theories is to investigate black hole solutions. It is particularly interesting to determine which properties of black holes deviate from those predicted by Einstein’s gravity and which properties remain robust features common to all higher-curvature modifications (Thomas, 2010; Clifton et al., 2012).

Obtaining black hole solutions for a generic theory where higher-curvature terms are treated perturbatively—as an effective theory—is relatively straightforward. In this approach, the solution can be viewed as an Einstein solution with correction terms arising from higher-curvature gravity. However, when the contribution from higher-curvature terms is non-perturbative, finding analytical solutions to the field equations becomes significantly more challenging. As a result, most of the black hole solutions are obtained numerically. In such cases, the resulting black hole solutions are not those of pure Einstein gravity, but rather solutions that incorporate both Einstein and higher-curvature gravity (Stelle, 1977; Sajadi et al., 2024; Salvio, 2018; Hamid, 2023; Sajadi et al., 2022; Banerjee et al., 2025; de Medeiros et al., 2024).

In this article, we employ the continued fraction expansion technique to derive static, spherically symmetric solutions for the theory with a generic coupling constant. The ansatz is constructed such that the coefficients in the continued fraction are determined by the behavior of the metric function near the event horizon. Then, the coefficients are matched with the asymptotic behavior at infinity. Unlike other expansions, which are valid only in a finite radius of convergence, continued fractions can remain accurate from the event horizon to spatial infinity. Another advantage of this method is its theory independence; that is, any gravitational theory can be studied by changing only the coefficients, while the general structure of the expansion is fixed. Despite its strengths, this method has some limitations; the accuracy of the solution depends on the number of coefficients considered in the expansion. Truncating the expansion introduces an error into the solution. The second limitation is that this method describes only the outside of the black hole with multiple horizons. This approach has recently been applied in various contexts (Konoplya and Zinhailo, 2019; Zinhailo, 2018; Rezzolla and Zhidenko, 2014). Obtaining analytic solutions allows us to study the thermodynamic properties and other characteristics of black hole solutions. In contrast, numerical solutions do not provide a clear understanding of the metric's dependence on the physical parameters of the system (Sajadi et al., 2020; Naseh Sajadi and Ponglertsakul, 2025; Naseh Sajadi et al., 2025; Sajadi and Hendi, 2022).

Moreover, in black hole physics, quasi-normal modes (QNMs) describe the characteristic oscillations of a perturbed black hole spacetime. These modes are exponentially damped by gravitational radiation, and their complex frequencies encode fundamental information about the black hole's parameters, such as mass, charge, and angular momentum. QNMs, thus, play a crucial role in black hole spectroscopy, allowing one to test general relativity and probe the nature of gravity in the strong-field regime through gravitational wave observations. From a theoretical perspective, QNMs have been extensively studied in the context of extremal or near-extremal black holes such as Kerr (Pong et al., 2020), Reissner–Nordström (Senjaya and Ponglertsakul, 2025), and anti-de Sitter (AdS) black holes. They are particularly relevant for exploring the transition between stability and instability in black hole spacetimes and understanding the near-horizon conformal symmetry predicted by the Kerr/CFT correspondence. Moreover, QNMs provide insight into the late-time tail behavior of perturbations and the dynamics of quantum fields near black hole horizons (Zimmerman and Mark, 2016; Berti et al., 2009; Kokkotas and Schmidt, 1999).

The article is organized as follows: In Section 2, we first review Einstein–quartic gravity. Then, we compute thermodynamic quantities and construct the first law and the Smarr formula. As a result, we obtain the solutions for the near-horizon quantities. In Subsection 2.1, we study the thermodynamic phase transition of a black hole. In Section 3, we obtain the metric function outside the black hole using a continued fraction expansion and study the stability of the black hole via computing its QNMs. Finally, we conclude the article in Section 4.

2 Basic formalism

The most general Lagrangian of Einstein–quartic gravity (EQG) can be written as follows (Sajadi et al., 2022; Ahmed et al., 2017; Khodabakhshi et al., 2020):

$$S = \frac{1}{16\pi G} \int d^4x \sqrt{-g} \left(\mathcal{R} - 2\Lambda - \sum_{i=1}^6 \tilde{\alpha}_i \widehat{\mathcal{L}}^i - \frac{1}{4} \mathcal{F}_{ab} \mathcal{F}^{ab} \right), \quad (1)$$

where $\mathcal{F}_{ab} = \partial_a A_b - \partial_b A_a$ is the electromagnetic tensor, $A_a = -q/r \delta_a^t$ is the gauge potential, $\widehat{\mathcal{L}}_i$ represents the quasi-topological Lagrangian densities, whose analytical expressions are given by Ahmed et al. (2017), Λ is the cosmological constant, and $\tilde{\alpha}_i$ represents the coupling constants of the theory.

Using the variational principle, one can find the following equation of motion:

$$\begin{aligned} \mathcal{E}_{ab} &= P_{acde} R_b{}^{cde} - \frac{1}{2} g_{ab} \mathcal{L} - 2 \nabla^c \nabla^d P_{acdb} - 2 T_{ab} = 0, \quad (2) \\ \nabla_a \mathcal{F}^{ab} &= 0, \quad P_{abcd} = \frac{\partial \mathcal{L}}{\partial R^{abcd}}, \quad T_{ab} = \mathcal{F}_{da} \mathcal{F}_b{}^d - \frac{1}{4} g_{ab} \mathcal{F}_{de} \mathcal{F}^{de}. \quad (3) \end{aligned}$$

Here, \mathcal{L} is the gravitational Lagrangian. We consider the following spherically symmetric and static line element for describing the geometry of spacetime:

$$ds^2 = -f(r) dt^2 + \frac{dr^2}{f(r)} + r^2 (d\theta^2 + \sin^2 \theta d\phi^2). \quad (4)$$

By inserting the line element in Equation 4 into the field in Equation 2 and integrating it, we obtain the following differential equation:

$$\begin{aligned} -(f-1)r + 2\mathcal{K} \left[\frac{ff'f''}{r^2} - \left(f - \frac{1}{2}rf' - 1 \right) + \frac{f^4}{8r} + \frac{f'^3}{6r^2} (f+2) + \frac{ff'^2}{r^3} (1-f) \right] \\ - 2M + \frac{q^2}{r} - \frac{\Lambda r^3}{3} = 0, \quad \mathcal{K} = -\frac{5}{6} \sum_{i=1}^6 \alpha_i. \quad (5) \end{aligned}$$

Here, M and q are integration constants related to mass and electric charge, respectively. The field in Equation 5 with respect to the function $f(r)$ is nonlinear. Therefore, we should solve it using approximation methods. First, we obtain the metric in the large r . In the large r limit, we expand the metric function as

$$f(r) = \Lambda_{eff} r^2 + \sum_{n=0} \frac{F_n}{r^n} = \Lambda_{eff} r^2 + F_0 + \frac{F_1}{r} + \frac{F_2}{r^2} + \dots, \quad (6)$$

where the effective cosmological constant Λ_{eff} satisfies

$$\Lambda_{eff} + \frac{1}{3} \Lambda + \frac{4}{3} \mathcal{K} \Lambda_{eff}^4 = 0. \quad (7)$$

The possible vacuum solutions of the theory have been discussed by Ahmed et al. (2017). By inserting the above expansions into the field from Equation 5 and solving order by order, one obtains Equation 8:

$$f(r) = \Lambda_{\text{eff}} r^2 + 1 - \frac{6M}{(3 + 16\mathcal{K}\Lambda_{\text{eff}}^3)r} + \frac{3q^2}{(3 + 16\mathcal{K}\Lambda_{\text{eff}}^3)r^2} + \frac{3024\mathcal{K}M^2\Lambda_{\text{eff}}^2}{(3 + 16\mathcal{K}\Lambda_{\text{eff}}^3)^3 r^4} + \dots \tag{8}$$

Then, we expand the function $f(r)$ around the event horizon r_+ as

$$f(r) = f_1(r - r_+) + f_2(r - r_+)^2 + f_3(r - r_+)^3 + \dots, \tag{9}$$

where f_i represents the expansion coefficients. Then, by inserting this expression into Equation 5 and expanding it, we obtain the following two equations from the zeroth and first orders of expansion:

$$r_+ - 2M + \frac{q^2}{r_+} + \frac{2\mathcal{K}f_1^3}{3r_+^2} + \frac{\mathcal{K}f_1^4}{4r_+} - \frac{\Lambda r_+^3}{3} = 0, \tag{10}$$

$$1 - f_1 r_+ - \Lambda r_+^2 + \frac{\mathcal{K}f_1^4}{12r_+^2} + \frac{2\mathcal{K}f_1^3}{3r_+^3} - \frac{q^2}{r_+^2} = 0. \tag{11}$$

By solving these equations, we find the following coefficients of expansion as¹

$$M = -\frac{r_+}{2} - \frac{\mathcal{K}f_1^4}{r_+} - \frac{8\mathcal{K}f_1^3}{3r_+^2}, \tag{12}$$

$$f_1 = \text{RootOf}(12r_+^3 - 12_Z r_+^4 - 12\Lambda r_+^5 + \mathcal{K}_Z r_+^4 + 8\mathcal{K}_Z r_+^3 - 12q^2 r_+). \tag{13}$$

From the higher-order terms in the expansion, the remaining coefficients can be obtained as follows:

$$f_3 = -\frac{1}{36\mathcal{K}r_+^2 f_1^2 (r_+ f_1 + 2)} (-5\Lambda r_+^5 - 76\mathcal{K}f_1^3 f_2 r_+^2 + 48\mathcal{K}f_1^2 f_2^2 r_+^3 + 29\mathcal{K}f_1^4 r_+ + 48\mathcal{K}f_1^3 + 48\mathcal{K}f_1 r_+^2 f_2^2 - 120\mathcal{K}f_1 f_2 r_+ + 5q^2 r_+ - 5f_1 r_+^4 - 5f_2 r_+^5). \tag{14}$$

f_2 is an undetermined expansion coefficient. The other constants are provided in Appendix A. Basically, f_1 has four branches of solutions. In the left panel of Figure 1, we show the behavior of the different branches using different colors. Because f_1 must be positive, only the blue and red branches are possible solutions. However, the red branch exhibits non-Einstein behavior for small positive \mathcal{K} ($\mathcal{K} \rightarrow 0^+$) and, thus, is excluded. Furthermore, for $\mathcal{K} \rightarrow 0^-$, the red branch does not reach $\mathcal{K} = 0$ and terminates at a negative finite \mathcal{K} before the general relativity (GR) point ($\mathcal{K} = 0$). Consequently, only the blue branch shows Einstein behavior in the small- \mathcal{K} limit and, therefore, remains as the physical branch of solution. In the right panel, we show the behavior of f_1 in terms of r_+ for positive and negative values of \mathcal{K} . The upper curve corresponds to a positive coupling constant, and the lower one to a negative coupling constant. For each event horizon radius, there are two positive $f_1 > 0$. The red upper curve can be considered a specific black hole solution of quartic theory, although the next section will show that this branch of solutions does not have a thermodynamic

phase transition. An explicit expression for f_1 corresponding to the blue branch is given by

$$f_1^{\text{ph}} = -\frac{2}{r_+} + \frac{\sqrt{2Z}}{2r_+} - \frac{\sqrt{W}}{2r_+}, \tag{15}$$

where

$$\begin{aligned} X &= -864 r_+^{10} \mathcal{K} + 864 r_+^8 \mathcal{K} q^2 + 864 r_+^{12} \mathcal{K} \Lambda - 576 r_+^6 \mathcal{K} q^4 - 1152 r_+^{10} \mathcal{K} q^2 \Lambda \\ &\quad - 576 r_+^{14} \mathcal{K} \Lambda^2 + 64 r_+^4 \mathcal{K} q^6 + 192 r_+^8 \mathcal{K} q^4 \Lambda + 192 r_+^{12} \mathcal{K} q^2 \Lambda^2 + 64 r_+^{16} \mathcal{K} \Lambda^3 \\ &\quad + 81 r_+^{16} + 2304 r_+^4 \mathcal{K}^2 - 4608 r_+^2 \mathcal{K}^2 q^2 - 4608 r_+^6 \mathcal{K}^2 \Lambda \\ &\quad + 2304 \mathcal{K}^2 q^4 + 4608 \mathcal{K}^2 q^2 r_+^4 \Lambda + 2304 r_+^8 \mathcal{K}^2 \Lambda^2, \\ Y &= -(-9 r_+^8 - 48 r_+^2 \mathcal{K} + 48 \mathcal{K} q^2 + 48 r_+^4 \mathcal{K} \Lambda - \sqrt{X}) \mathcal{K} r_+, \\ Z &= \frac{8\mathcal{K}^3 \sqrt{Y} + Y^{2/3} r_+ + 12\mathcal{K} r_+^5 - 4\mathcal{K} r_+^3 q^2 - 4\mathcal{K} r_+^7 \Lambda}{\mathcal{K}^3 \sqrt{Y}}, \\ W &= 32 - \frac{2r_+ Y^{1/3}}{\mathcal{K}} - \frac{24r_+^5}{3\sqrt{Y}} - \frac{8r_+^3 q^2}{3\sqrt{Y}} + \frac{8r_+^7 \Lambda}{3\sqrt{Y}} + \frac{12\sqrt{2} r_+^6}{\mathcal{K} \sqrt{Z}} - \frac{64\sqrt{2}}{\sqrt{Z}}. \end{aligned} \tag{16}$$

Next, we determine the physical range of the relevant quantities. To this end, we introduce dimensionless constants as

$$x_+ = \frac{r_+}{2M}, \quad \widehat{f}_1 = M f_1, \quad Q = \frac{q}{M}, \quad \widehat{\mathcal{K}} = \frac{\mathcal{K}}{M^6}, \quad \widehat{\Lambda} = \Lambda M^2. \tag{17}$$

Hence, Equations 10, 11 in a dimensionless form take the following form:

$$2x_+ - 2 + \frac{Q^2}{2x_+} + \frac{\widehat{\mathcal{K}} \widehat{f}_1^3}{6x_+^2} + \frac{\widehat{\mathcal{K}} \widehat{f}_1^4}{8x_+} - \frac{8\widehat{\Lambda} x_+^3}{3} = 0, \tag{18}$$

$$1 - 2\widehat{f}_1 x_+ - 4\widehat{\Lambda} x_+^2 + \frac{\widehat{\mathcal{K}} \widehat{f}_1^4}{48x_+^2} + \frac{\widehat{\mathcal{K}} \widehat{f}_1^3}{12x_+^3} - \frac{Q^2}{4x_+^2} = 0. \tag{19}$$

Then, we solve the above equations for x_+ and \widehat{f}_1 in terms of other dimensionless quantities. We do not include the explicit expressions here as they are very lengthy; instead, we present the numerical behavior of the quantities in Figures 2, 3, 4. Figures 2, 3 show a three-dimensional plot of the dimensionless horizon radius $r_+/2M$ and dimensionless surface gravity $M f_1^2$ as a function of the charge to mass ratio q/M and the dimensionless coupling \mathcal{K}/M^6 . These figures also display that for every value of negative couplings $\widehat{\mathcal{K}} < 0$ and $|Q| < 1$, there is one horizon with positive $\widehat{f}_1 > 0$. However, for $1 < Q < Q_{\text{max}}$ and $\widehat{\mathcal{K}} < -3/4$, there are two real solutions with positive $\widehat{f}_1 > 0$ (this can be observed from the left panel of Figure 4). We can also see from the following expansions that the deviation from the extremality happens for $\widehat{\mathcal{K}} < -3/4$.

$$Q = 1 - \frac{1}{8} \widehat{f}_1^2 - \left(\frac{1}{4} + \frac{\widehat{\mathcal{K}}}{3} \right) \widehat{f}_1^3 + \mathcal{O}(\widehat{f}_1^4), \tag{20}$$

$$x_+ = \frac{1}{2} + \frac{1}{4} \widehat{f}_1 + \frac{1}{4} \widehat{f}_1^2 + \left(\frac{5}{16} - \frac{\widehat{\mathcal{K}}}{3} \right) \widehat{f}_1^3 + \mathcal{O}(\widehat{f}_1^4). \tag{21}$$

As shown in the analysis of the quartic gravity coupled to nonlinear electrodynamics by Sajadi et al. (2022), this indicates

1 RootOf is a command used as a placeholder for roots of equations in MapleSoft (1980).

2 Surface gravity is a measure of the gravitational acceleration felt at the event horizon of a black hole, that is, surface gravity = $f_1/2$.

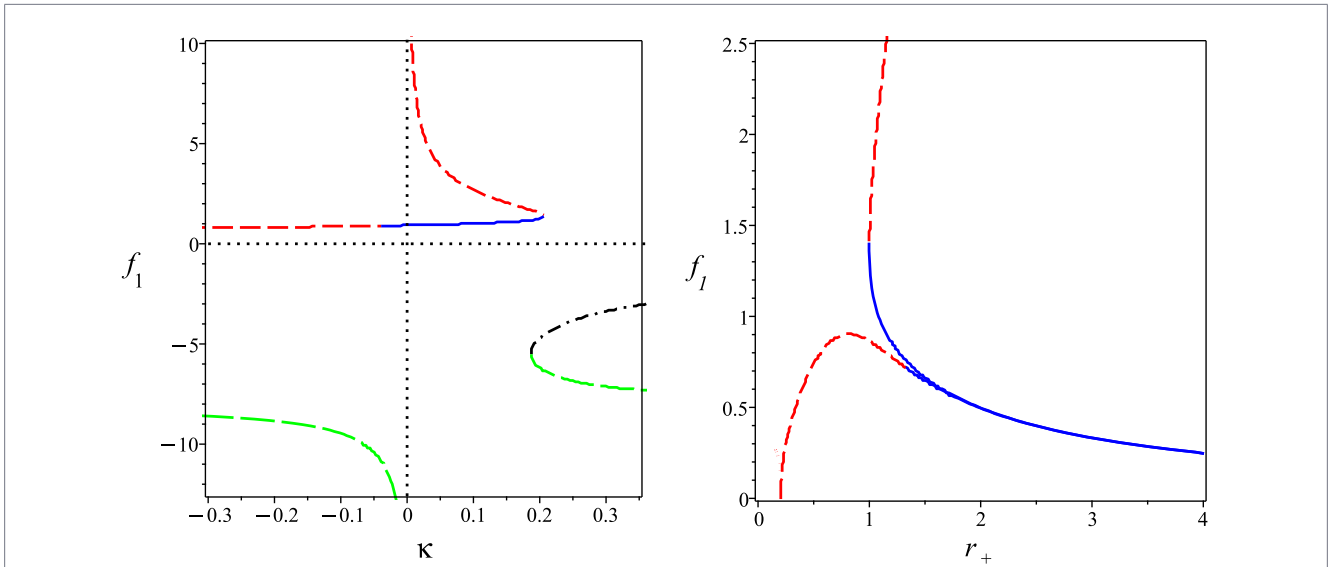


FIGURE 1 Behavior of f_1 in terms of K (left) and r_+ (right) for $\Lambda = 0$, $q = 0.2$. In the right panel, the upper curves correspond to $K = 0.2$, and the lower curves correspond to $K = -0.2$.

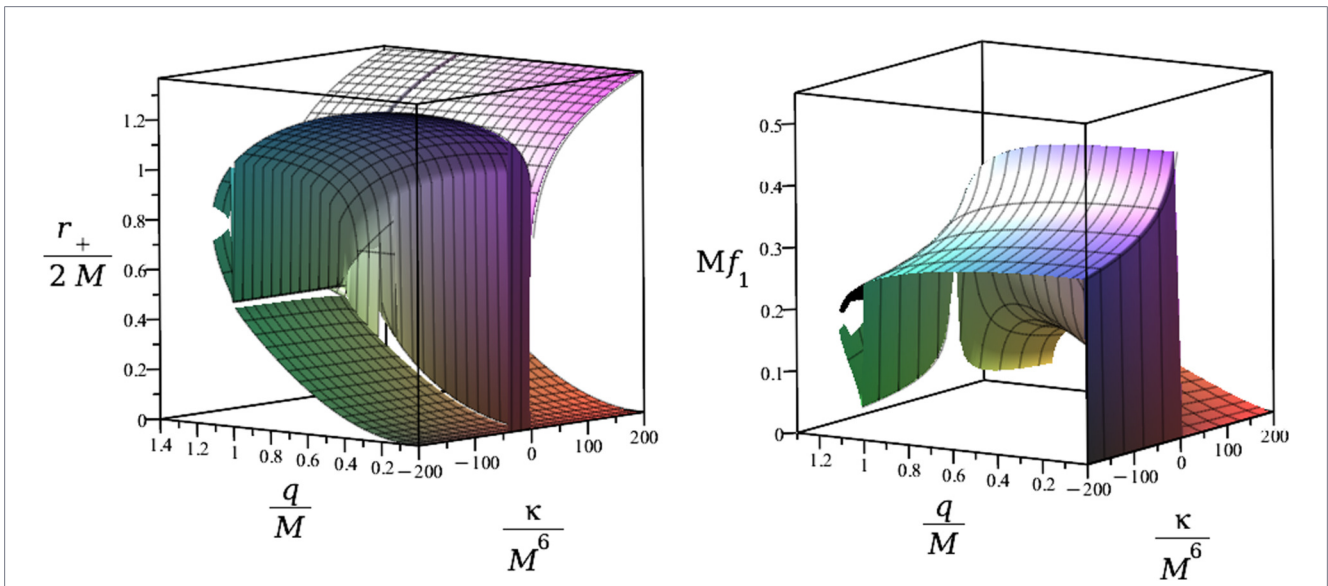
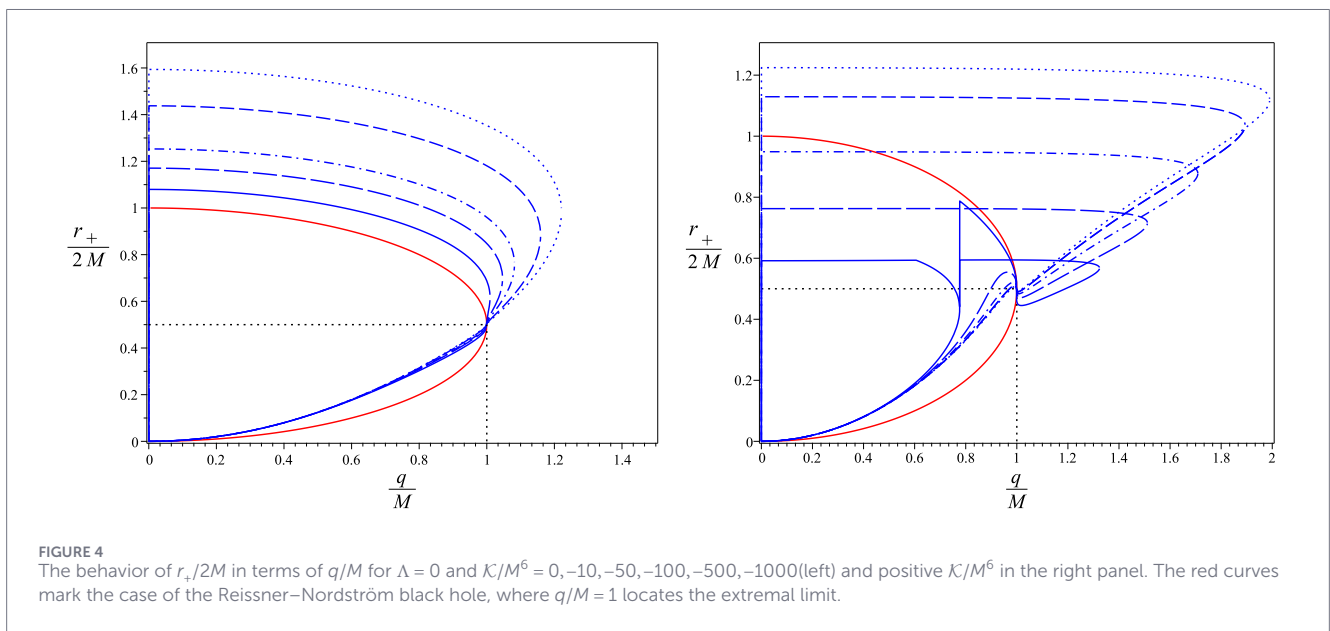
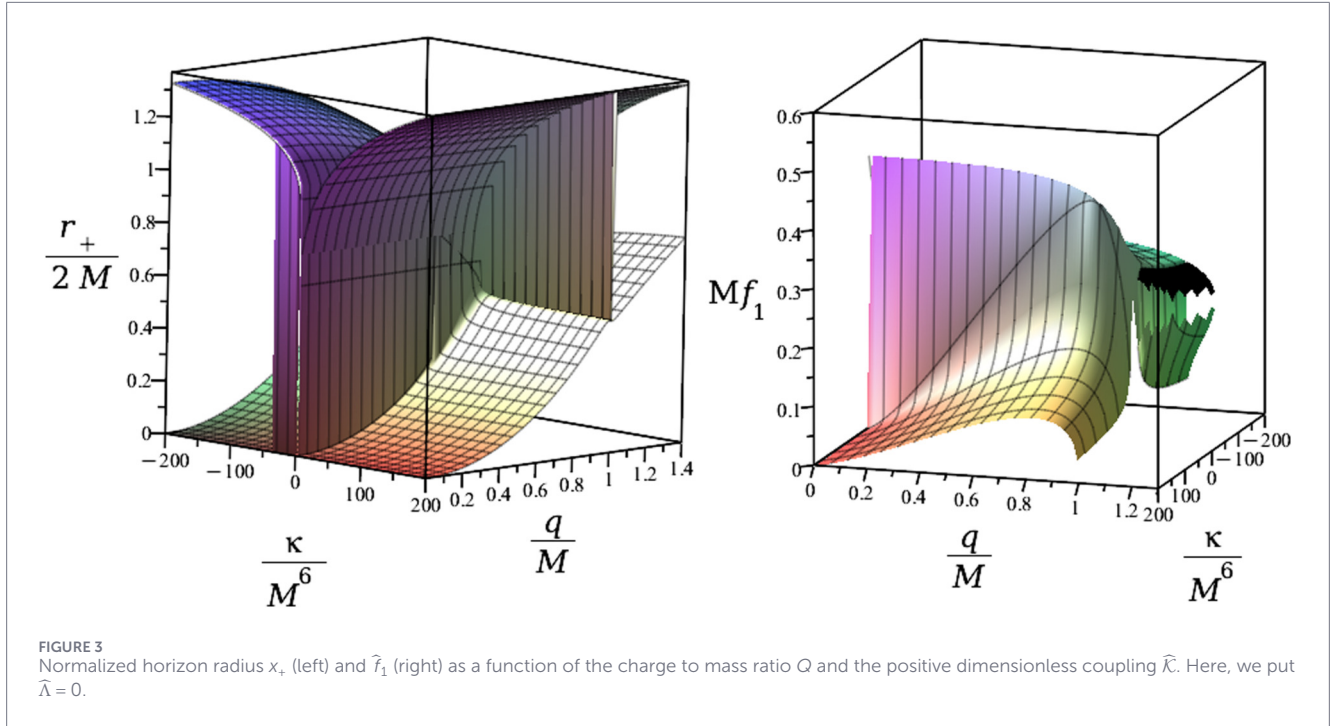


FIGURE 2 Normalized horizon radius x_+ (left) and \hat{f}_1 (right) as a function of the charge to mass ratio Q and the negative dimensionless coupling $\hat{\kappa}$. Here, we put $\hat{\Lambda} = 0$.

that charged black holes in EQG are not required to satisfy the Einstein–Maxwell extremality bound. **Figure 3** demonstrates that, for a positive coupling constant, only a single horizon with positive surface gravity exists. Moreover, for $Q > 1$ and $\hat{\kappa} > 0$, no horizon is present for any positive value of the coupling constant (see the right panel of **Figure 4**). In the next section, we show that the black hole solutions associated with this branch ($\hat{\kappa} > 0$) are thermodynamically stable in the large black hole but do not exhibit any thermodynamic phase transitions.

In the following, to study the thermodynamics of the black hole in the extended phase space, we treat the bare cosmological constant (Λ) as a thermodynamic variable (not Λ_{eff}). This means that the asymptotic behavior of the metric in **Equation 8** does not affect our thermodynamical quantities. For a static spacetime, the temperature is defined as

$$T = \left. \frac{f'(r)}{4\pi} \right|_{r_+} = \frac{f_1(r_+, q, \Lambda, \mathcal{K})}{4\pi}. \tag{22}$$



We compute the entropy as follows (Wald, 1993; Iyer and Wald, 1994):

$$S = -2\pi \int_{Horizon} d^2x \sqrt{\eta} \frac{\delta L}{\delta R_{abcd}} \epsilon_{ab} \epsilon_{cd} = \pi r_+^2 + \frac{2\pi \mathcal{K} f_1^2(r_+, q, \Lambda, \mathcal{K}) (3 + r_+ f_1(r_+, q, \Lambda, \mathcal{K}))}{3r_+^2}. \quad (23)$$

The chemical potential associated with the electric charge, the cosmological constant, and the coupling constant of theory \mathcal{K} is given as follows (see Appendix C):

$$\psi_q = \frac{q}{r_+}, \quad \psi_\Lambda = \frac{r_+^3}{6} + Y', \quad \psi_{\mathcal{K}} = -\frac{f_1^3(r_+, q, \Lambda, \mathcal{K}) (4 + r_+ f_1(r_+, q, \Lambda, \mathcal{K}))}{24r_+^2} + Y. \quad (24)$$

In the above equations, we assume $Y = Y(r_+, q, \Lambda, \mathcal{K})$, $Y' = Y'(r_+, q, \Lambda, \mathcal{K})$, and we determine them so that the following conditions are met:

$$\frac{\partial^2 f_1}{\partial q \partial \Lambda} = \frac{\partial^2 f_1}{\partial \Lambda \partial q}, \quad \frac{\partial^2 f_1}{\partial r_+ \partial \Lambda} = \frac{\partial^2 f_1}{\partial \Lambda \partial r_+}, \quad \frac{\partial^2 f_1}{\partial q \partial r_+} = \frac{\partial^2 f_1}{\partial r_+ \partial q}, \quad \frac{\partial^2 f_1}{\partial q \partial \mathcal{K}} = \frac{\partial^2 f_1}{\partial \mathcal{K} \partial q}, \dots \quad (25)$$

Thus, we obtain

$$Y = \frac{h\left(\frac{\mathcal{K}}{r_+^6}\right)}{r_+^5}, \quad Y' = c' r_+^3, \quad (26)$$

with some arbitrary dimensionless function $h(\mathcal{K}/r_+^6)$. Without loss of generality, we may set $c' = 0$. Physically, $\psi_{\mathcal{K}}$ and ψ_{Λ} are interpreted as the thermodynamic volumes associated with \mathcal{K} and Λ , respectively (Xiao et al., 2025). We now consider the thermodynamics of these black hole solutions, whose basic equations are the first law and the Smarr formula.

$$dM = TdS + \psi_q dq + \psi_{\Lambda} d\Lambda + \psi_{\mathcal{K}} d\mathcal{K}, \quad (27)$$

$$M = 2TS + 6\mathcal{K}\psi_{\mathcal{K}} + q\psi_q + 2\psi_{\Lambda}\Lambda. \quad (28)$$

From Equation 28, we obtain

$$M = \frac{1}{2}f_1(r_+, q, \Lambda, \mathcal{K})r_+^2 + \frac{f_1^4(r_+, q, \Lambda, \mathcal{K})\mathcal{K}}{12r_+} + \frac{6\mathcal{K}}{r_+^5}h\left(\frac{\mathcal{K}}{r_+^6}\right) + \frac{\Lambda r_+^3}{3} + \frac{q^2}{r_+}, \quad (29)$$

yielding the mass parameter as $M(r_+, \mathcal{K}, \Lambda, q)$. We now impose the first law (Equation 27), which becomes

$$\begin{aligned} \frac{\partial M}{\partial r_+} dr_+ + \frac{\partial M}{\partial \mathcal{K}} d\mathcal{K} + \frac{\partial M}{\partial \Lambda} d\Lambda + \frac{\partial M}{\partial q} dq &= T \frac{\partial S}{\partial r_+} dr_+ + T \frac{\partial S}{\partial \mathcal{K}} d\mathcal{K} + T \frac{\partial S}{\partial \Lambda} d\Lambda \\ &+ T \frac{\partial S}{\partial q} dq + \psi_{\mathcal{K}} d\mathcal{K} - \psi_{\Lambda} d\Lambda + \psi_q dq. \end{aligned} \quad (30)$$

To solve the above differential equations, we adopt, for simplicity, the ansatz: $h\left(\frac{\mathcal{K}}{r_+^6}\right) = m\left(\frac{\mathcal{K}}{r_+^6}\right)^n$ with some numbers m and n . Comparing each coefficient yields the following first-order differential equations:

$$\begin{aligned} \frac{\partial M}{\partial r_+} - T \frac{\partial S}{\partial r_+} = 0, \Rightarrow 0 &= \frac{1}{2} \frac{\partial f_1}{\partial r_+} r_+^2 + \frac{1}{2} r_+ f_1 - \frac{\mathcal{K} f_1^3}{6r_+} \frac{\partial f_1}{\partial r_+} + \frac{1}{12} \frac{f_1^4 \mathcal{K}}{r_+^2} + \frac{f_1^3 \mathcal{K}}{r_+^3} \\ &- \frac{\mathcal{K} f_1^2}{r_+^2} \frac{\partial f_1}{\partial r_+} - 6m(6n+5) \left(\frac{\mathcal{K}}{r_+^6}\right)^{n+1} + \Lambda r_+^2 - \frac{q^2}{r_+^2}, \end{aligned} \quad (31)$$

$$\begin{aligned} \frac{\partial M}{\partial \mathcal{K}} - T \frac{\partial S}{\partial \mathcal{K}} - \psi_{\mathcal{K}} = 0, \Rightarrow 0 &= \frac{1}{2} \frac{\partial f_1}{\partial \mathcal{K}} r_+^2 - \frac{f_1^3 \mathcal{K}}{6r_+} \frac{\partial f_1}{\partial \mathcal{K}} - \frac{f_1^4}{24r_+} - \frac{\mathcal{K} f_1^2}{r_+^2} \frac{\partial f_1}{\partial \mathcal{K}} - \frac{f_1^3}{3r_+^2} \\ &+ \frac{m(6n+5)}{r_+^5} \left(\frac{\mathcal{K}}{r_+^6}\right)^n, \end{aligned} \quad (32)$$

$$\frac{\partial M}{\partial \Lambda} - T \frac{\partial S}{\partial \Lambda} + \psi_{\Lambda} = 0, \Rightarrow 0 = -\frac{\mathcal{K} f_1^3}{6r_+} \frac{\partial f_1}{\partial \Lambda} - \frac{\mathcal{K} f_1^2}{r_+^2} \frac{\partial f_1}{\partial \Lambda} + \frac{1}{2} \frac{\partial f_1}{\partial \Lambda} r_+^2 + \frac{r_+^3}{2}, \quad (33)$$

$$\frac{\partial M}{\partial q} - T \frac{\partial S}{\partial q} - \psi_q = 0, \Rightarrow 0 = -\frac{\mathcal{K} f_1^3}{6r_+} \frac{\partial f_1}{\partial q} - \frac{\mathcal{K} f_1^2}{r_+^2} \frac{\partial f_1}{\partial q} + \frac{r_+^2}{2} \frac{\partial f_1}{\partial q} + \frac{q}{r_+}. \quad (34)$$

By solving differential Equations 31–34, one can obtain a solution for f_1 as follows:

$$\begin{aligned} f_1(r_+, q, \Lambda, \mathcal{K}) = \text{RootOf} \left[-24(6n+5)m\mathcal{K} \left(\frac{\mathcal{K}}{r_+^6}\right)^n - 12(n+1)r_+^3 (\Lambda r_+^5 \right. \\ \left. + _Z r_+^4 + 2c_1 r_+^3 + \left(q^2 - \frac{\mathcal{K} _Z^4}{12}\right)r_+ - \frac{2 _Z^3 \mathcal{K}}{3}) \right], \end{aligned} \quad (35)$$

Here, c_1 is an integration constant, and $_Z$ is a global variable. For $m = 0$ and $\mathcal{K} \rightarrow -12/5\mathcal{K}$, Equation 35 coincides with Equation 12, which is obtained before using the near-horizon expansion. This means that, to obtain the same results, the pure gauge term in Equation 24 must vanish. For nonzero m , the thermodynamic quantities obtained from the first law and the Smarr formula differ from those derived using the field equations. Now, we can put f_1 in the thermodynamic quantities. At first, by substituting Equation 35 into the temperature in Equation 22, one can obtain

$$\begin{aligned} T = \text{RootOf} \left[-24(6n+5)m\mathcal{K} \left(\frac{\mathcal{K}}{r_+^6}\right)^n - 12(n+1)r_+^3 (\Lambda r_+^5 + _Z r_+^4 + 2c_1 r_+^3 \right. \\ \left. + \left(q^2 - \frac{\mathcal{K} _Z^4}{12}\right)r_+ - \frac{2 _Z^3 \mathcal{K}}{3}) \right]. \end{aligned} \quad (36)$$

In the limit $\mathcal{K} \ll 1$ and $m = n = 0$, we obtain

$$T \approx -\frac{c_1}{2\pi r_+} - \frac{\Lambda r_+}{4\pi} - \frac{q^2}{4\pi r_+^3} + \mathcal{O}(\mathcal{K}). \quad (37)$$

To obtain the standard Schwarzschild temperature at the leading order, we set $c_1 = -1/2$.

One gets extremal conditions by setting the temperature to 0. For non-perturbative f_1 , this yields

$$q_{\text{ext}} = \sqrt{1 - \Lambda r_+^2} r_+, \quad (38)$$

which is independent of \mathcal{K} . By substituting Equation 35 into Equation 29, one can obtain the Arnowitt–Deser–Misner (ADM) mass of the black hole as

$$\begin{aligned} M = \frac{r_+}{2} - \frac{\Lambda r_+^3}{6} + \frac{q^2}{2r_+} + \frac{\mathcal{K}}{3r_+^2} \text{RootOf}(\mathcal{K} _Z^4 r_+ - 12\Lambda r_+^5 - 12 _Z r_+^4 \\ + 8\mathcal{K} _Z^3 - 12q^2 r_+ + 12r_+^3)^3 + \frac{\mathcal{K}}{8r_+} \text{RootOf}(\mathcal{K} _Z^4 r_+ \\ - 12\Lambda r_+^5 - 12 _Z r_+^4 + 8\mathcal{K} _Z^3 - 12q^2 r_+ + 12r_+^3)^4. \end{aligned} \quad (39)$$

By imposing the extremal condition $f_1 = 4\pi T = 0$ in Equation 29 and using Equation 38, the extremal mass is obtained as follows:

$$M_{\text{ext}} = \frac{r_+}{3} + \frac{2q^2}{3r_+}. \quad (40)$$

In the small \mathcal{K} limit, the physical branch of ADM mass becomes

$$M \approx \frac{r_+}{2} + \frac{q^2}{2r_+} - \frac{\Lambda r_+^3}{6} + \frac{(q^2 + \Lambda r_+^4 - r_+^2)^3 (3q^2 + 3\Lambda r_+^4 - 11r_+^2)}{24r_+^3} \mathcal{K} + \mathcal{O}(\mathcal{K}^2). \quad (41)$$

In the above expression, the leading order term corresponds to the Reissner–Nordström–AdS black hole in Einstein’s gravity. The next leading order term (with the \mathcal{K}) is the correction term from the quartic gravity. Moreover, as shown in Figure 4 and in the results of Equations 38, 40, the extremal condition is independent of \mathcal{K} and coincides with that of Einstein gravity. This is because the near-horizon geometry does not receive corrections from the higher-curvature terms; the near-horizon metric $AdS_2 \times S^2$ remains unchanged. While far away from the horizon, in the bulk, the geometry receives corrections from the higher curvature.

This reflects the fact that extremality is determined by the near-horizon geometry rather than by the dynamics of the theory. Similar behavior has been observed in Lovelock and cubic quasi-topological gravities, where higher-curvature terms modify non-extremal black holes while leaving the extremal relation unchanged (Cano and Pereñiguez, 2020; Micol Frassino and Rocha, 2020; Robert, 2010). Therefore, this is not counterintuitive for the theory. Substituting Equation 35 into Equation 23, the black hole entropy is explicitly obtained:

$$S = \pi r_+^2 + \frac{2\pi\mathcal{K}}{3r_+} \text{RootOf}(\mathcal{K}r_+Z^4 - 12\Lambda r_+^5 - 12r_+^4Z + 8\mathcal{K}Z^3 - 12q^2r_+ + 12r_+^3)^3 + \frac{2\pi\mathcal{K}}{r_+^2} \text{RootOf}(\mathcal{K}r_+Z^4 - 12\Lambda r_+^5 - 12r_+^4Z + 8\mathcal{K}Z^3 - 12q^2r_+ + 12r_+^3)^2. \tag{42}$$

In the small \mathcal{K} limit, the physical branch is given as

$$S \approx \pi r_+^2 - \frac{2\pi(q^2 + \Lambda r_+^4 - r_+^2)(q^2 + \Lambda r_+^4 - 4r_+^2)}{3r_+^{10}} \mathcal{K} + \mathcal{O}(\mathcal{K}^2). \tag{43}$$

The presence of negative terms in the above expansion signals that the entropy becomes negative below a critical horizon radius. By setting the entropy equal to 0, one obtains a bound for the event horizon radius in the small q regime as follows:

$$S = 0 \quad \rightarrow \quad r_+ \approx q + \frac{\Lambda}{2}q^3 \pm \frac{3}{4}\sqrt{\frac{1}{-2\mathcal{K}}}q^4 + \mathcal{O}(q^7). \tag{44}$$

As observed for negative $\mathcal{K} < 0$ and in the vicinity of the extremal point, the entropy becomes negative. This negativity is associated with the non-Einstein branch of solutions, indicating that this branch is a ghost branch and, therefore, non-physical (Dykaar et al., 2017; Hennigar and Mann, 2017). The chemical potential corresponding to the coupling of the theory, in the small \mathcal{K} limit, is given by

$$\psi_{\mathcal{K}} = \frac{(q^2 + \Lambda r_+^4 - r_+^2)(5r_+^2 - q^2 - \Lambda r_+^4)}{24r_+^{13}} + \frac{\mathcal{K}}{72r_+^{25}}(q^2 + \Lambda r_+^4 - r_+^2)^5(q^2 - 9r_+^2 + \Lambda r_+64)(q^2 + \Lambda r_+^4 - 4r_+^2) + \mathcal{O}(\mathcal{K}^2). \tag{45}$$

The Gibbs free energy in terms of q , Λ , and \mathcal{K} is given by

$$G = M - TS = \frac{1}{4}f_1r_+^2 - \frac{\mathcal{K}}{12r_+}f_1^4 - \frac{\mathcal{K}}{2r_+^2}f_1^3 + \frac{\Lambda r_+^3}{3} + \frac{q^2}{r_+} + \frac{6\mathcal{K}m}{r_+^5}\left(\frac{\mathcal{K}}{r_+^6}\right)^n. \tag{46}$$

By substituting Equation 35 into Equation 46, at the limit of small \mathcal{K} , one can obtain

$$G \approx \frac{r_+}{4} + \frac{\Lambda r_+^3}{12} + \frac{3q^2}{4r_+} + \frac{(q^2 + \Lambda r_+^4 - r_+^2)^3\mathcal{K}}{48r_+^{13}}(5q^2 + 5\Lambda r_+^4 - 13r^2 + 32r_+^2 - 8q^2 - 8\Lambda r_+^4) + \mathcal{O}(\mathcal{K}^2).$$

To address the local thermodynamic stability of the black hole, we consider the heat capacity:

$$C = T\left(\frac{\partial S}{\partial T}\right)_{\Lambda, \mathcal{K}} = \frac{2\pi f_1}{r_+^3 \partial_{r_+} f_1} \left(r_+ \mathcal{K} f_1 (2 + r_+ f_1) \partial_{r_+} f_1 + r_+^4 - 2\mathcal{K} f_1^2 - \frac{1}{3} \mathcal{K} r_+ f_1^3 \right). \tag{47}$$

At the limit $\mathcal{K} \rightarrow 0$, the heat capacity becomes

$$C = -\frac{2\pi r_+^2(q^2 + \Lambda r_+^4 - r_+^2)}{3q^2 - \Lambda r_+^4 - r_+^2} - \frac{\pi(q^2 + r_+^4\Lambda - r_+^2)^2\mathcal{K}}{3r_+^{10}(3q^2 - \Lambda r_+^4 - r_+^2)^2} (66q^6 + 40q^4r_+^4\Lambda - 303q^4r_+^2 - 22q^2r_+^8\Lambda^2 - 18q^2r_+^6\Lambda + 248q^2r_+^4 + 4r_+^{12}\Lambda^3 - 3r_+^{10}\Lambda^2 + 10\Lambda r_+^8 - 59r_+^6) + \mathcal{O}(\mathcal{K}^2). \tag{48}$$

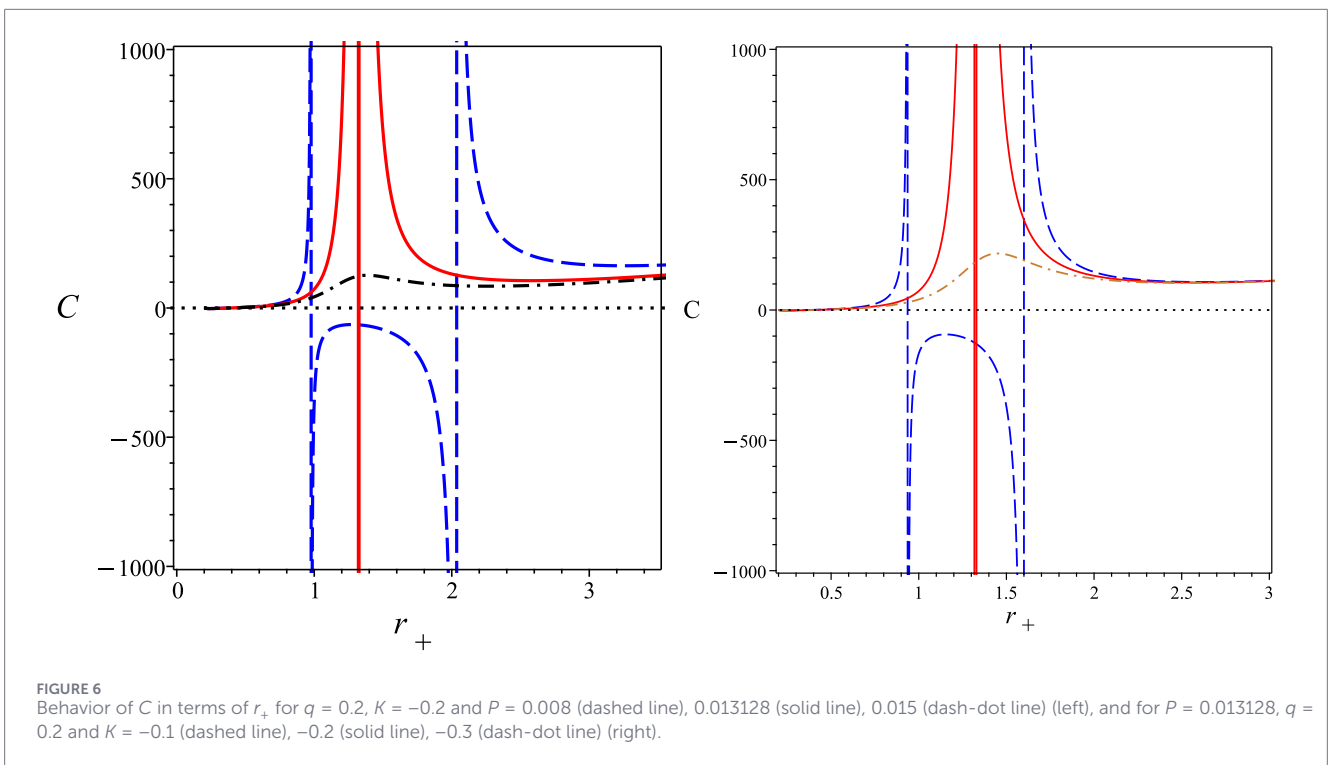
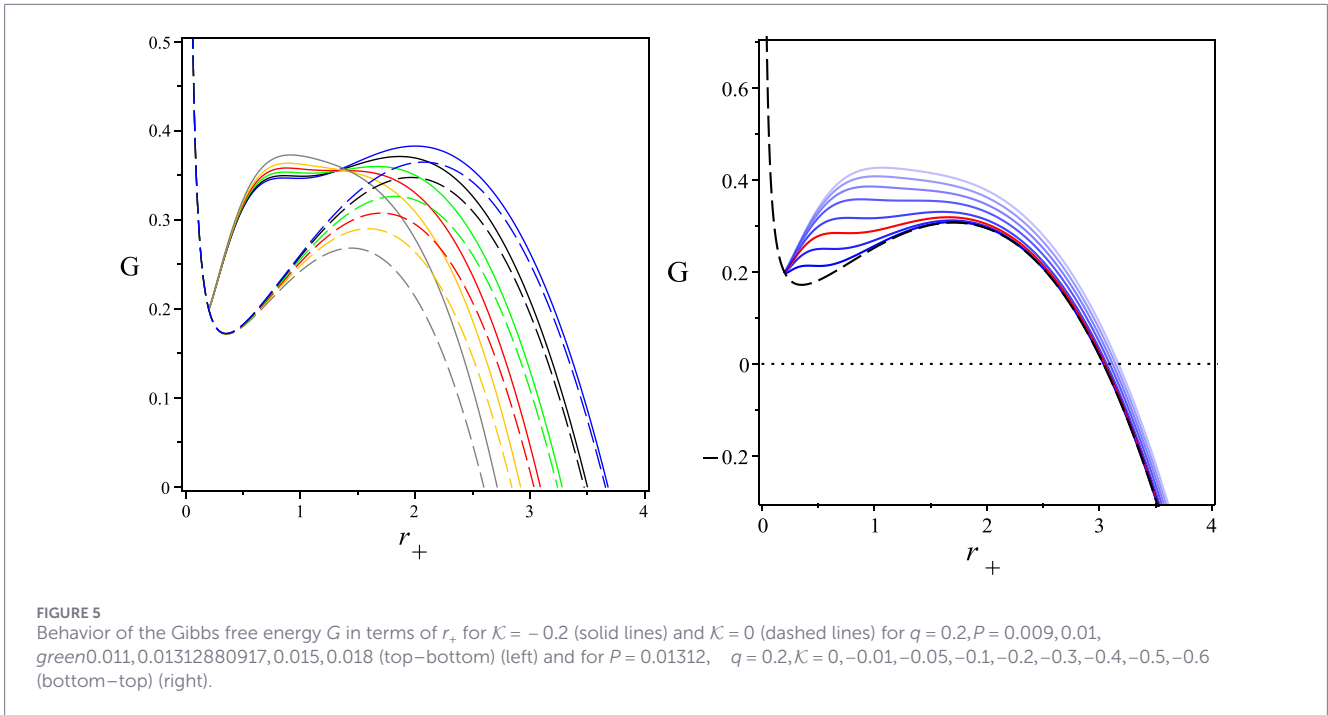
In the next section, we will study thermodynamic stability and phase transitions.

2.1 Phase transition and stability

Thermodynamic stability characterizes how a system in thermodynamic equilibrium responds to fluctuations in its thermodynamic parameters. It is important to distinguish between global and local stability. In a globally stable system, the system can exchange energy with a thermodynamic reservoir while remaining in equilibrium. The preferred phase of the system is the one that minimizes the Gibbs free energy. Therefore, the behavior of the Gibbs free energy is used to analyze global stability (Hendi et al., 2016a; Hendi et al., 2016b; Hendi and Momennia, 2015; Momennia and Hendi, 2021). In Figure 5, we present the Gibbs free energy as a function of r_+ . From the left panel of Figure 5, we observe that for constant \mathcal{K} and q , the Gibbs free energy decreases with entropy S for both small and large event horizons, while it increases for intermediate values. This behavior indicates that intermediate black holes are globally unstable. Because large black holes possess negative Gibbs free energy, they are more stable than small black holes. Moreover, Figure 5 illustrates that increasing the pressure ($-8\pi P = \Lambda$) enhances the stability of the black hole. In Figure 5b, the Gibbs free energy is shown as a function of r_+ for constant pressure and electric charge. It is evident that as \mathcal{K} increases, the black hole becomes less stable.

On the other hand, local stability concerns how the system responds to small perturbations in its thermodynamic parameters. To study the thermodynamic stability of black holes under small variations in the thermodynamic coordinates, one can examine the behavior of the heat capacity (C). The positivity of the heat capacity ensures local stability (Quevedo, 2007; Quevedo, 2008; Quevedo and Sanchez, 2008; Hossein Hendi and Momennia, 2018). The behavior of C is plotted in Figure 6a. As shown in the figure, three distinct regions exist for $P < P_c = 0.013128$. The partially positive specific heat in the small and large black hole regions indicates that these black holes are thermodynamically locally stable. In contrast, the negative specific heat in the intermediate black hole region corresponds to a locally unstable phase. At the critical pressure $P = P_c$, the unstable region disappears, and the heat capacity exhibits a divergence. For $P > P_c$, C remains positive with no divergence, implying that the black hole is locally stable for all values of r_+ . In Figure 6b, the dependence of C on r_+ for different values of the parameter \mathcal{K} is shown. It is evident that at the critical pressure, increasing \mathcal{K} eliminates the critical point, leading to a fully stable black hole configuration.

The behavior of the heat capacity can also indicate the occurrence of phase transitions. The heat capacity exhibits at most two divergences, which separate small stable black holes, an intermediate unstable region with a medium horizon radius, and large stable black holes. These divergences coincide with the



extremum points of the temperature and the Gibbs free energy. The plot of the Gibbs free energy as a function of temperature displays a characteristic swallowtail structure, as shown in Figure 7. When $P < P_c$, the Gibbs free energy develops a swallowtail-like shape, signaling a small/large black hole first-order phase transition analogous to the liquid–gas phase transition in a van der Waals fluid. At the critical pressure $P = P_c$, the swallowtail structure disappears, corresponding to the critical point.

By solving Equation 11, for $\Lambda = -8\pi P$, one can obtain the equation of state as follows:

$$P = \frac{T}{2r_+} - \frac{1}{8\pi r_+^2} + \frac{q^2}{8\pi r_+^4} - \frac{8\pi^2 T^3 \mathcal{K}}{3r_+^5} (\pi r_+ T + 2). \quad (49)$$

The resulting equation of state is nonlinear in temperature. This nonlinear temperature dependence appears to be a generic feature of black hole solutions in generalized quasi-topological theories

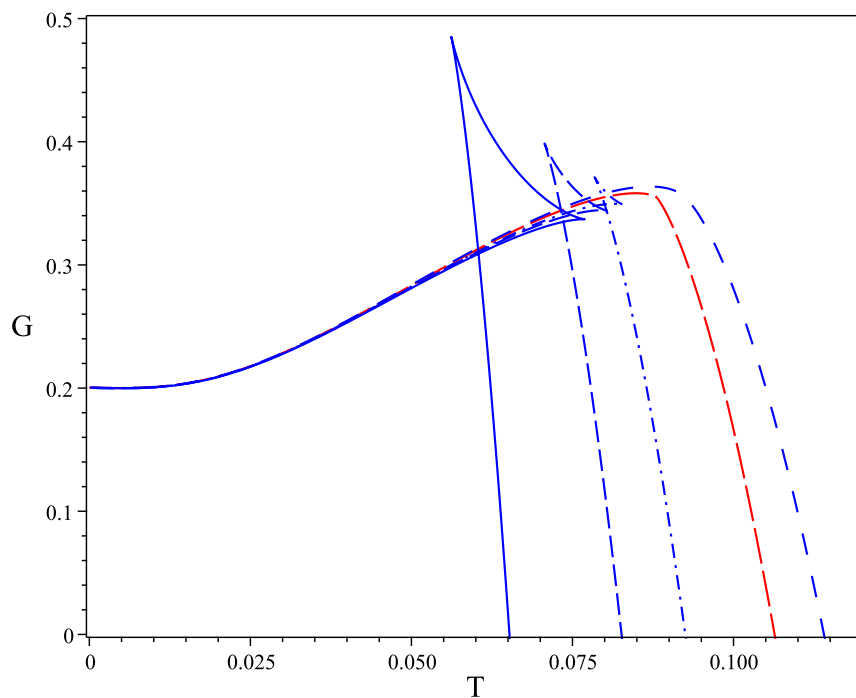


FIGURE 7 Behavior of F in terms of T for $q = 0.2, \mathcal{K} = -0.2$ and $P = 0.005, 0.01, 0.08, 0.0131288, 0.015$ (left to right).

(Ahmed et al., 2017). This deviation from ideal gas behavior, for generic \mathcal{K} , occurs at small r_+ and can be interpreted as a signal of quantum interactions. For $\mathcal{K} \rightarrow 0$, the last terms vanish, reducing the solution to a charged AdS black hole in Einstein gravity. For $\mathcal{K} < 0$, the last term becomes positive, which allows a phase transition in the system. For $\mathcal{K} > 0$, a phase transition may occur only for sufficiently small values of $\mathcal{K} \ll q$. For a neutral black hole $q = 0$ and $\mathcal{K} < 0$, the equation of state (Equation 49) admits a single critical point:

$$\left. \frac{\partial P}{\partial r_+} \right|_T = 0, \quad \left. \frac{\partial^2 P}{\partial r_+^2} \right|_T = 0, \quad (50)$$

with the corresponding critical values given by

$$r_c = \frac{\sqrt{23}^{\frac{5}{6}} (4\sqrt{2} - \sqrt{7})^{\frac{1}{3}} (-\mathcal{K})^{\frac{1}{6}}}{3},$$

$$T_c = \frac{(9 + 2\sqrt{14}) \sqrt{23}^{\frac{1}{6}}}{4(4\sqrt{2} - \sqrt{7})^{\frac{1}{3}} (-\mathcal{K})^{\frac{1}{6}} \pi (11 + 3\sqrt{14})}, \quad (51)$$

$$P_c = \frac{3(425049 + 116272\sqrt{14}) 3^{\frac{1}{3}}}{32\pi(1106079 + 295612\sqrt{14}) (-\mathcal{K}(39 - 8\sqrt{14}))^{\frac{1}{3}}}.$$

The ratio of these values is (Kubiznak and Robert, 2012; Hossein Hendi et al., 2016)

$$\frac{P_c r_c}{T_c} = \frac{3(9668963 + 2584139\sqrt{14})}{8(18231847 + 4872666\sqrt{14})} = 0.1988751392, \quad (52)$$

which is independent of the parameters of the black hole solution and thus constitutes a universal quantity for black holes in this theory ($q = 0$). It should be noted that the critical quantities, taken separately, are functions of the black hole and theory parameters; however, the ratio (Equation 52) is independent of any parameters

and is, therefore, universal. Figure 8 illustrates the behavior of the pressure as a function of the event horizon radius, with T , q , and \mathcal{K} held fixed. The temperature of the isotherms decreases from top to bottom. The upper solid blue curve corresponds to the ideal gas phase, the solid red curve denotes the critical isotherm, and the lower solid blue curve represents a temperature below the critical temperature, where the pressure becomes 0 ($T_0 = 0.07217801561, r_+ = 0.8050806533$). This behavior is similar to the pressure–volume diagram of the van der Waals liquid–gas system. By performing a numerical analysis for $q = 0.2$ and $\mathcal{K} = -0.2$, we find the critical quantities $P_c = 0.01312880917$, $r_c = 1.323249339$, and $T_c = 0.08797792346$. These results are consistent with Figures 6, 7, 8. Using these results, the universal ratio is obtained as $P_c r_c / T_c = 0.197466448$, and it is different from that of a van der Waals fluid ($3/16 = 0.1875$). This deviation is directly related to the presence of $1/r_+^5$ in the quartic corrections in the equation of state (Equation 49).

3 Metric function

Now, we want to obtain an approximate analytic solution that is valid near the horizon and at large r . Here, we employ a continued fraction expansion (Rezzolla and Zhidenko, 2014). To obtain the metric function using continued fraction expansion, we must first determine the near-horizon coefficient f_1 and the asymptotic expansion coefficient F_1 (Equation 6). In the previous section, we determined them explicitly in two ways: first, by using the first two near-horizon expansions of the field equations and second, by using the first law of thermodynamics and the Smarr formula. Then, the results of the two ways are compared.

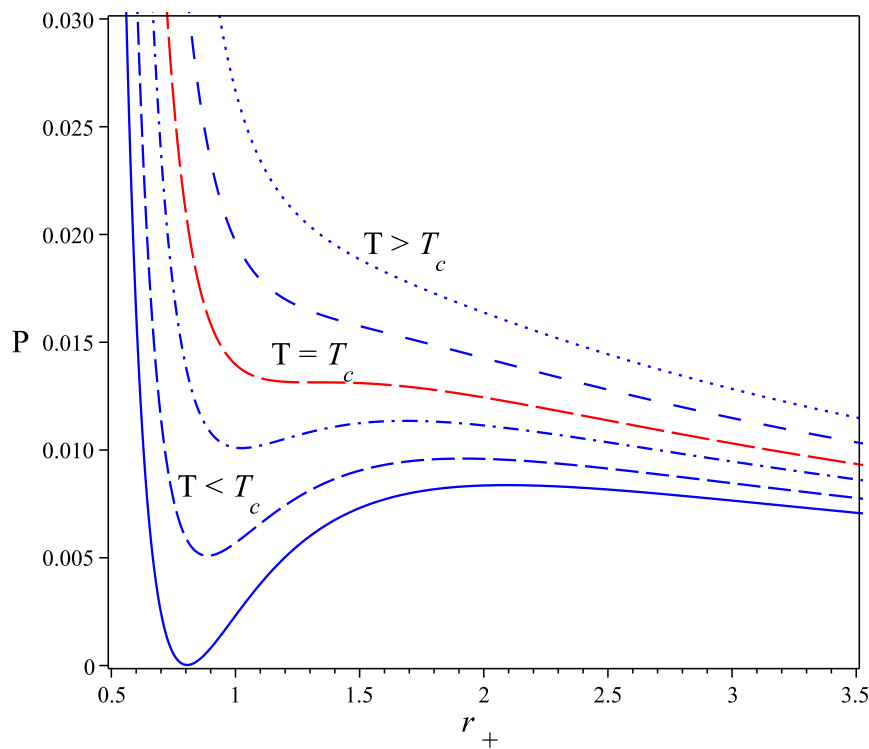


FIGURE 8 Behavior of P in terms of r_+ for $q = 0.2, \mathcal{K} = -0.2$ and $T = 0.0722, 0.077, 0.085, 0.088, 0.09, 0.1$ (bottom–top).

With f_1 and $F_1 = -2M$ in hand from Equation 35 or Equation 12, the full metric can now be determined using a continued fraction expansion (Konoplya and Zinhailo, 2019; Zinhailo, 2018). To achieve this, we write

$$f(r) = xA(x), x = 1 - \frac{r_+}{r}, \tag{53}$$

with

$$A(x) = 1 - \epsilon(1-x) + (a_0 - \epsilon)(1-x)^2 + \frac{a_1(1-x)^3}{1 + \frac{a_2x}{1 + \frac{a_3x}{1 + \dots}}} \tag{54}$$

The continued fraction is truncated at order 4. By expanding Equation 53 near the horizon ($x \rightarrow 0$) and the asymptotic region ($x \rightarrow 1$), we obtain

$$\epsilon = -\frac{F_1}{r_+} - 1, \quad a_0 = \frac{q^2}{r_+^2}, \quad a_1 = -1 - a_0 + 2\epsilon + r_+f_1, \tag{55}$$

for the lowest order expansion coefficients, with the remaining a_i given in terms of (r_+, q) and f_2 ; we provide these expressions in Appendix B. Because the field equations do not determine f_2 , its value must be manually input into the continued fraction. There are different methods to fix f_2 . The first is to demand a consistent Einstein gravity limit for the near-horizon expansion. The second method is to consider the metric function written in continued fraction expansion (Equation 53). If we are going to keep the fractions to f_n , we do so by setting $f_{n+1} = 0$. Because all f_n ($n > 2$) are functions of f_2 , the equation $f_{n+1} = 0$ can be solved to find an approximate value for f_2 . For instance, in the case that we keep the fraction to f_4 , we can solve $f_5 = 0$ to find f_2 . In this work, we use the second method to determine f_2 . The result is an approximate analytic solution for the metric functions everywhere outside the

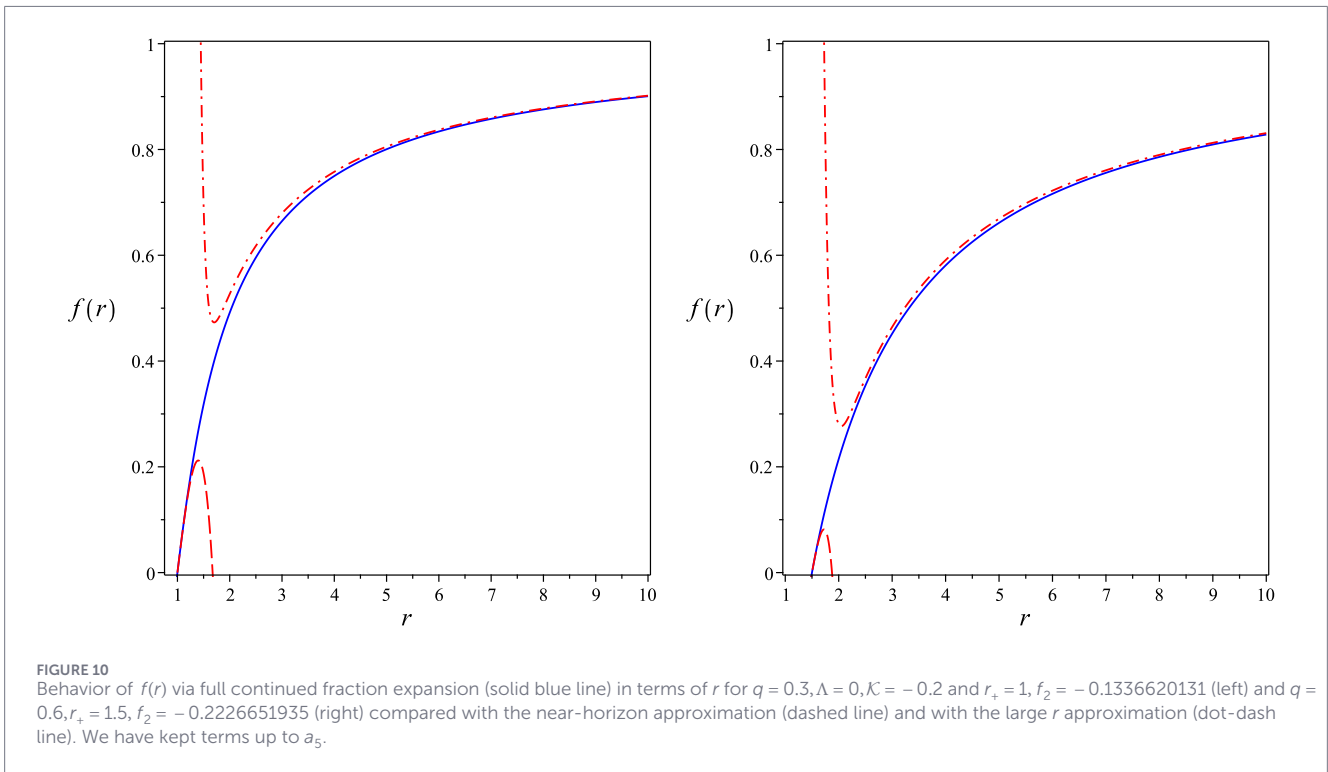
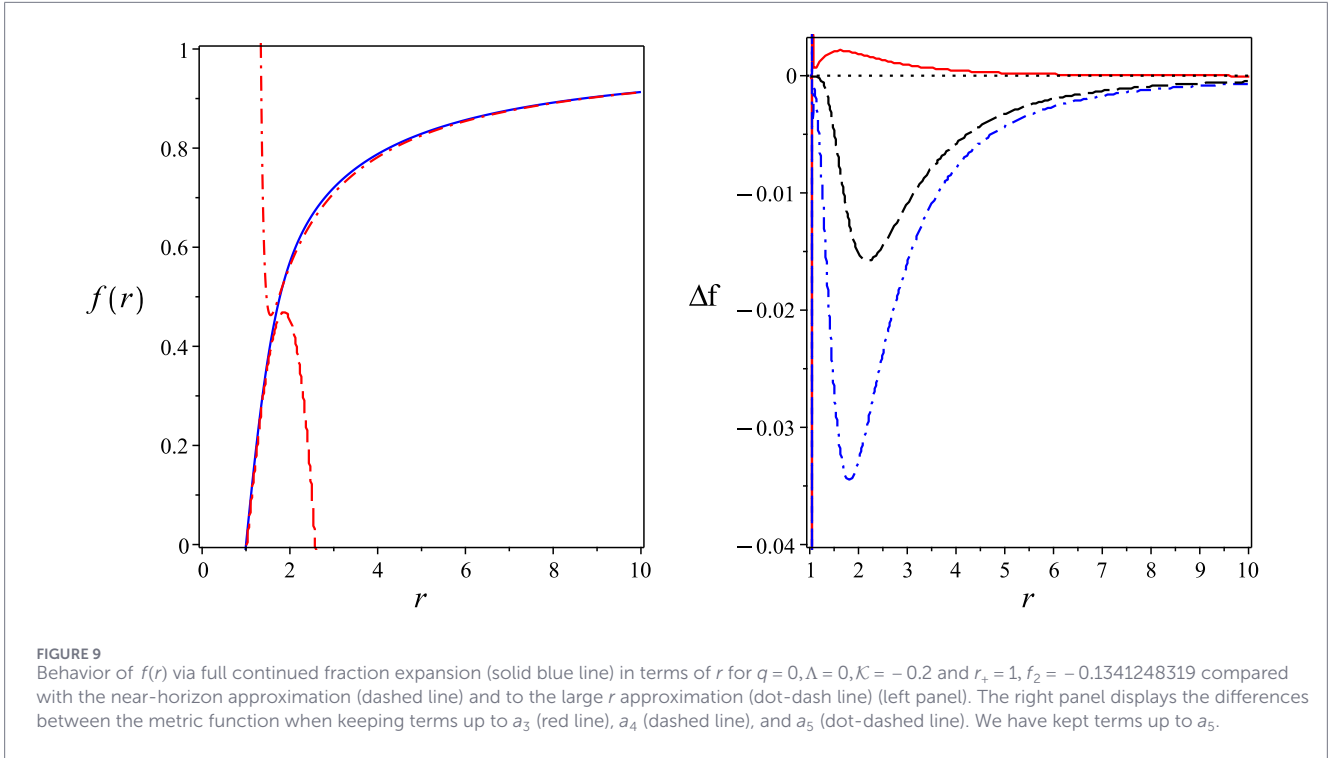
horizon. In Figure 9, we present the solution for $f(r)$, depicting the full continued fraction solution (Equation 53) along with its comparison to the near-horizon and large r series expansion. The latter is given by dot-dashed lines. We observe that the continued fraction expansion converges to both of these other approximations. We also show the difference between the metric functions in the right panel when we keep different terms in the expansion. The blue solid line is the difference between $f(r, a_2) - f(r, a_3)$, the dashed black line is $f(r, a_3) - f(r, a_4)$, and dot-dashed line is $f(r, a_4) - f(r, a_5)$. As observed, as the terms in the continued fraction expansion increase, the differences decrease.

Figure 10 shows the metric function of the charged black hole through the continued fraction expansion for different radii of the event horizon and different charges. In addition, we have compared the full solution with the large- r and near-horizon solutions. Good agreement between the solutions is again clearly visible.

In the following, we consider the dynamical stability of a black hole using quasi-normal modes. Gravitational perturbations are more directly relevant to black hole stability in higher-curvature theories; nevertheless, here, we consider scalar perturbations as they provide early evidence for the stability of our solution. We consider a massless scalar field Φ propagating in a black hole background governed by the Einstein–quartic theory. Its evolution obeys the massless Klein–Gordon equation:

$$\square\Phi = 0. \tag{56}$$

To solve the above Klein–Gordon equation analytically, it is convenient to use the following standard separation of variables by making use of the spherical harmonic



functions, (Y_{lm})

$$\Phi(t, r, \theta, \phi) = \sum_{lm} \frac{1}{r} \varphi_l(r) Y_{lm}(\theta, \phi) e^{i\omega t}. \quad (57)$$

Accordingly, the Klein–Gordon equation can be simplified as the Schrodinger-type equation as follows:

$$(\partial_{r^*}^2 + \omega^2 - U_l(r)) \varphi_l(r^*) = 0, \quad (58)$$

where the effective potential is given by

$$U_l(r(r^*)) = f \left(\frac{l(l+1)}{r^2} + \frac{f'}{r} \right), \quad r^* = \int \frac{dr}{f(r)}, \quad (59)$$

where l is the spherical harmonic index and r^* is the tortoise coordinate. The metric function here is obtained from the full continued fraction expansion. The effective potential for several angular momentum numbers l and both neutral and charged black

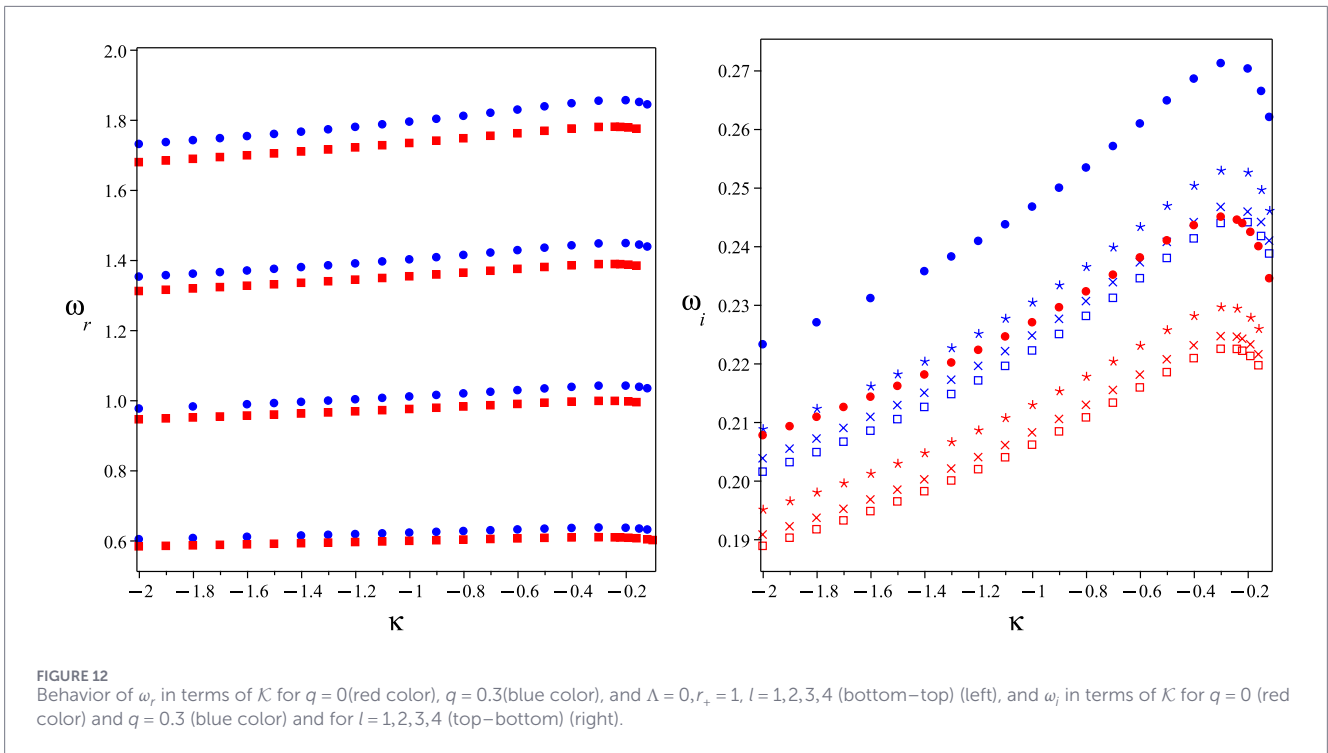
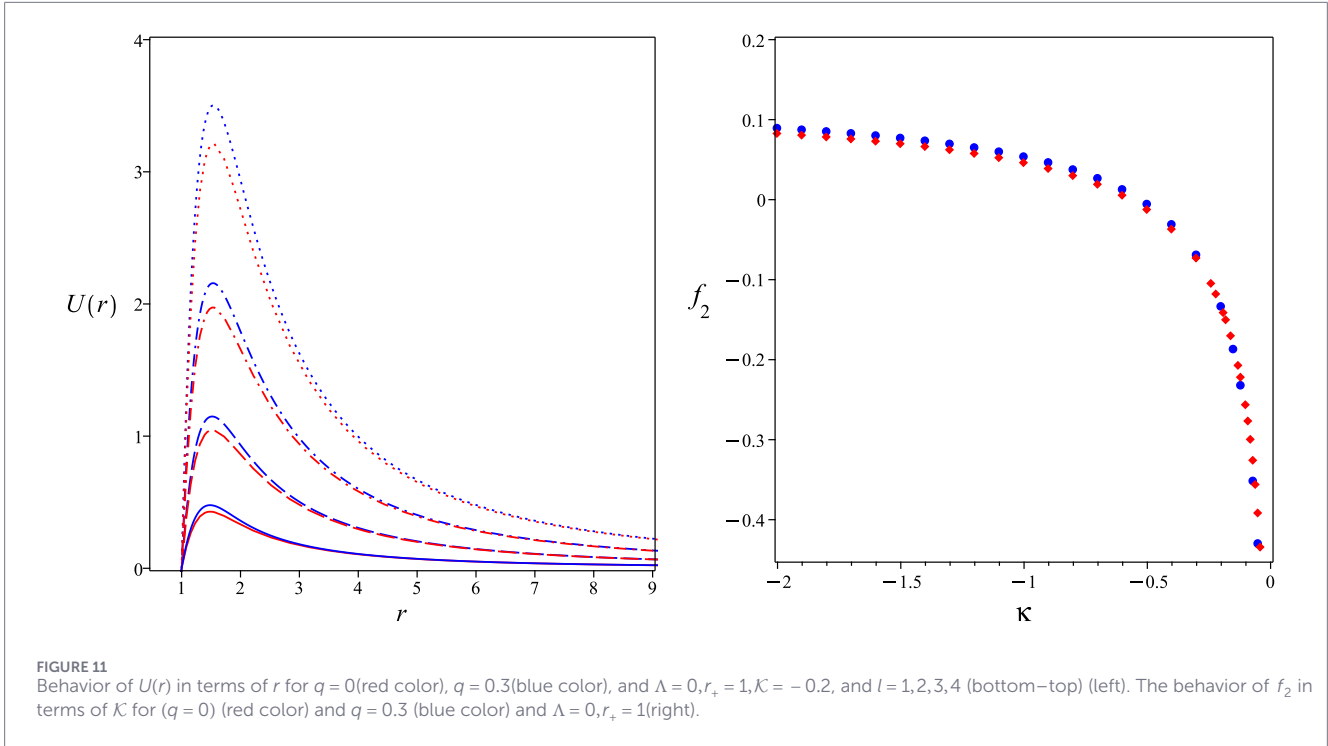


TABLE 1 Numerical values of f_2 , ω_r , and ω_i are determined by considering different truncations of the continued fraction expansion for $\mathcal{K} = -0.2$, $l = 1, r_+ = 1$, $q = 0$.

Truncation term	f_2	ω_r	ω_i
3	-0.3169585188	0.606091139	0.2127379883
4	-0.2664607039	0.6090929446	0.2170631127
5	-0.1575633974	0.6241053897	0.252134987
6	-0.1341248319	0.6360372337	0.2703193668
7	-0.1271730749	0.6485843937	0.2680549076

holes has been shown in the left panel of Figure 11. The potential forms a single barrier outside the event horizon, similar to the case in Schwarzschild and Reissner–Nordström geometries, and vanishes at the horizon ($r^* \rightarrow -\infty (r = r_+ = 1)$) and spatial infinity ($r^* \rightarrow \infty$)³. As l increases, the height of the potential barrier increases, pushing the peak rightward. This is expected because a higher l corresponds to a stronger centrifugal term $l(l+1)/r^2$. Introducing the electric charge increases the barrier height and broadens the potential barrier for all values of l . Near the black hole and large l , the potential is more modified because of the repulsive effect of the electric charge and centrifugal term. In the right panel of Figure 11, we have displayed the numerical value of f_2 as a function of \mathcal{K} . Higher-curvature corrections reduce the value of f_2 . In the following, we have used f_2 from the figure mentioned to obtain the QNM frequencies. To compute quasi-normal frequencies, we follow the method described by Ferrari and Mashhoon (1984) (see Appendix D for a review). This method provides a semi-analytical way to determine quasi-normal frequencies. It has been implemented in several studies on black holes' quasi-normal modes (Naseh Sajadi et al., 2025; Pong et al., 2020; Ponglertsakul et al., 2018).

In Figure 12, we illustrate the behavior of the quasi-normal frequency with respect to the \mathcal{K} for both $q=0$ (red color) and $q=0.3$ (blue color). The left panel shows that the real part of the frequency increases with the \mathcal{K} , angular momentum, and electric charge, and this leads to faster oscillations of the perturbation. The right panel shows that the imaginary part of the frequency is positive⁴. Thus, it can be concluded that the black hole is linearly stable. With increasing l , the values of the imaginary part of the

frequencies decrease. Including the electric charge increases the imaginary part and, therefore, damps the perturbation more quickly. Similar trends are observed for the Reissner–Nordström black holes in Einstein gravity (Ferrari and Mashhoon, 1984). In addition, these figures shows that, as \mathcal{K} increases, ω_i first increases, then reaches a maximum, and finally decreases. This means that for a specific value of \mathcal{K} , the perturbations are absorbed by the black hole. Physically, the peak in the imaginary part of the quasi-normal frequency comes from a competition between two effects: around $\mathcal{K} \approx -0.3$, the effective potential barrier becomes sharper, which increases the escape of perturbations, while near $\mathcal{K} \approx 0$, the barrier becomes shallower, leading to a reduced decay rate.

Table 1 shows the numerical values of f_2 , together with the real and imaginary parts of the frequency, obtained by truncating the continued fraction expansion at different orders. As the truncation order increases, the changes in f_2 become smaller, signaling the onset of convergence of the continued fraction method. In contrast, the quantities ω_r and ω_i display a smoother dependence on the truncation order and approach stable values more rapidly. This suggests that the quasi-normal mode frequencies are less sensitive to the truncation than the coefficient f_2 .

4 Conclusion

In this work, we have constructed an approximate analytical solution for a charged black hole in Einstein–quartic gravity using the continued fraction expansion method. Starting from the near-horizon and asymptotic expansions, we smoothly connected these regimes to obtain an analytic expression for the metric function that remains valid throughout the exterior region of the black hole. The solution agrees well with both limits, showing that the continued fraction method is trustworthy in higher-curvature gravity.

We have verified the first law of black hole thermodynamics and the Smarr relation, explicitly showing how quartic curvature corrections modify the mass, entropy, temperature, and other thermodynamic quantities. The thermodynamic analysis reveals the existence of van der Waals-type phase transitions between small and large black holes. The critical quantities are determined, and the universal ratio $P_c r_c / T_c$ is found to be independent of the model parameters, indicating a generic feature of the theory.

Moreover, the study of local and global stability shows that large black holes are both locally and globally stable, while intermediate black holes are unstable below the critical pressure. The quasi-normal mode analysis confirms the dynamical stability of spacetime and illustrates how the quartic coupling affects the oscillation frequencies.

Overall, our results establish a consistent analytic framework for exploring black holes in the Einstein–quartic gravity. The continued fraction expansion is a useful tool for studying black holes in higher-curvature theories and can be extended to rotating, higher-dimensional, or dynamical cases.

Data availability statement

The original contributions presented in the study are included in the article/supplementary material; further inquiries can be directed to the corresponding author.

³ For asymptotically AdS spacetime $\Lambda < 0$, the effective potential diverges at the AdS boundary, while it reaches zero at the horizon. The important consequence of this reflective boundary is that the waves cannot escape to infinity. Instead, perturbations bounce back and forth between the boundary and the black hole, leading to long-lived modes because energy cannot leak to infinity, and damping is controlled only by absorption at the horizon. Therefore, the imaginary parts of QNMs are smaller than in asymptotically flat spacetime. Moreover, the real part of the frequency of the QNMs is affected by the AdS boundary for a large black hole ($r_+ > \sqrt{-3/\Lambda}$) (Horowitz and Hubeny, 2000).

⁴ Here, positive ω_i corresponds to a stable black hole because we have chosen the time-component signature in Equation 57 to be positive ($\Phi = e^{+i\omega t}$).

Author contributions

SP: Conceptualization, Supervision, Validation, Writing – review and editing. SS: Conceptualization, Investigation, Software, Validation, Writing – original draft.

Funding

The author(s) declared that financial support was received for this work and/or its publication. This research has received funding support from the National Student Research Forum (NSRF) via the Program Management Unit for Human Resource and Institutional Development, Research, and Innovation grant number \$B13F680083\$.

Conflict of interest

The author(s) declared that this work was conducted in the absence of any commercial or financial relationships that could be construed as a potential conflict of interest.

References

- Ahmed, J., Hennigar, R. A., Mann, R. B., and Mir, M. (2017). Quintessential quartic quasi-topological quartet. *JHEP* 05, 134. doi:10.1007/jhep05(2017)134
- Banerjee, A., Pradhan, A., Sakalli, I., and Dixit, A. (2025). Properties of interacting quark star in light of rastall gravity. *Cl. Quant. Grav.* 42 (2), 025008. doi:10.1088/1361-6382/ad9c0f
- Berti, E., Cardoso, V., and Starinets, A. O. (2009). Quasinormal modes of black holes and black branes. *Cl. Quant. Grav.* 26, 163001. doi:10.1088/0264-9381/26/16/163001
- Cano, P. A., and Pereñiguez, D. (2020). Extremal rotating black holes in Einsteinian cubic gravity. *Phys. Rev. D.* 101 (4), 044016. doi:10.1103/physrevd.101.044016
- Clifton, T., Ferreira, P. G., Padilla, A., and Skordis, C. (2012). Modified gravity and cosmology. *Phys. Rept.* 513, 1–189. doi:10.1016/j.physrep.2012.01.001
- de Medeiros, W. P. F., Lazo, M. J., Müller, D., and Sales, D. A. (2024). Tilt in quadratic gravity. *Eur. Phys. J. C* 84 (8), 843. doi:10.1140/epjc/s10052-024-13171-0
- Dykaar, H., Hennigar, R. A., and Mann, R. B. (2017). Hairy black holes in cubic quasi-topological gravity. *JHEP* 05, 045. doi:10.1007/jhep05(2017)045
- Ferrari, V., and Mashhoon, B. (1984). New approach to the quasinormal modes of a black hole. *Phys. Rev. D.* 30, 295–304. doi:10.1103/physrevd.30.295
- Hamid, R. B. (2023). Charged rotating black strings in Einsteinian quartic gravity. *Nucl. Phys. B* 987, 116083. doi:10.1016/j.nuclphysb.2023.116083
- Hendi, S. H., and Momennia, M. (2015). Thermodynamic instability of topological black holes with nonlinear source. *Eur. Phys. J. C* 75 (2), 54. doi:10.1140/epjc/s10052-015-3283-2
- Hendi, S. H., Panahiyan, S., and Momennia, M. (2016a). Extended phase space of AdS black holes in einstein-gauss-bonnet gravity with a quadratic nonlinear electrodynamics. *Int. J. Mod. Phys. D.* 25 (06), 1650063. doi:10.1142/s0218271816500632
- Hendi, S. H., Panahiyan, S., Eslam Panah, B., and Momennia, M. (2016b). Thermodynamic instability of nonlinearly charged black holes in gravity's rainbow. *Eur. Phys. J.* 76 (3), 150. doi:10.1140/epjc/s10052-016-3994-z
- Hennigar, R. A., and Mann, R. B. (2017). Black holes in Einsteinian cubic gravity. *Phys. Rev. D.* 95 (6), 064055. doi:10.1103/physrevd.95.064055
- Quevedo, H. (2007). Geometrothermodynamics. *J. Math. Phys.* 48, 013506. doi:10.1063/1.2409524
- Horowitz, G. T., and Hubeny, V. E. (2000). Quasinormal modes of AdS black holes and the approach to thermal equilibrium. *Phys. Rev. D.* 62, 024027. doi:10.1103/physrevd.62.024027
- Hossein Hendi, S., and Momennia, M. (2018). AdS charged black holes in einstein-yang-mills gravity's rainbow: thermal stability and PV criticality. *Phys. Lett. B* 777, 222–234. doi:10.1016/j.physletb.2017.12.033

Generative AI statement

The author(s) declared that generative AI was not used in the creation of this manuscript.

Any alternative text (alt text) provided alongside figures in this article has been generated by Frontiers with the support of artificial intelligence and reasonable efforts have been made to ensure accuracy, including review by the authors wherever possible. If you identify any issues, please contact us.

Publisher's note

All claims expressed in this article are solely those of the authors and do not necessarily represent those of their affiliated organizations, or those of the publisher, the editors and the reviewers. Any product that may be evaluated in this article, or claim that may be made by its manufacturer, is not guaranteed or endorsed by the publisher.

- Hossein Hendi, S., Panahiyan, S., Panah, B. E., Faizal, M., and Momennia, M. (2016). Critical behavior of charged black holes in gauss-bonnet gravity's rainbow. *Phys. Rev. D.* 94 (2), 024028. doi:10.1103/physrevd.94.024028
- Iyer, V., and Wald, R. M. (1994). Some properties of noether charge and a proposal for dynamical black hole entropy. *Phys. Rev. D.* 50, 846–864. doi:10.1103/physrevd.50.846
- Khodabakhshi, H., Giaimo, A., and Mann, R. B. (2020). Einstein quartic gravity: shadows, signals, and stability. *Phys. Rev. D.* 102 (4), 044038. doi:10.1103/physrevd.102.044038
- Kokkotas, K. D., and Schmidt, B. G. (1999). Quasinormal modes of stars and black holes. *Living Rev. rel.* 2 (2), 2. doi:10.12942/lrr-1999-2
- Konoplya, R. A., and Zinhailo, A. F. (2019). Hawking radiation of non-Schwarzschild black holes in higher derivative gravity: a crucial role of grey-body factors. *Phys. Rev. D.* 99 (10), 104060. doi:10.1103/physrevd.99.104060
- Kubiznak, D., and Robert, B. (2012). Mann-P-V criticality of charged AdS black holes. *JHEP*, 07:033. doi:10.1007/JHEP07(2012)033
- Maplesoft (1980). Mathematics-based software & services for education, engineering, and research. Available online at: <https://www.maplesoft.com/support/help/Maple/view.aspx?path=RootOf> (Accessed March 9, 2026).
- Micol Frassinio, A., and Rocha, J. V. (2020). Charged black holes in Einsteinian cubic gravity and nonuniqueness. *Phys. Rev. D.* 102 (2), 024035. doi:10.1103/physrevd.102.024035
- Momennia, M., and Hendi, S. H. (2021). Critical phenomena and reentrant phase transition of asymptotically Reissner-Nordström black holes. *Phys. Lett. B* 822, 136692. doi:10.1016/j.physletb.2021.136692
- Naseh Sajadi, S., and Ponglertsakul, S. (2025). Superradiance of charged static black hole in cubic gravity. *Eur. Phys. J. Plus* 140 (6), 565. doi:10.1140/epjp/s13360-025-06459-x
- Naseh Sajadi, S., and Ponglertsakul, S. (2025). More on analytically approximate solution to quadratic gravity. *Ann. Phys.* 477, 170007. doi:10.1016/j.aop.2025.170007
- Ponglertsakul, S., and Gwak, B. (2020). Massive scalar perturbations on myers-perry-de Sitter black holes with a single rotation. *Eur. Phys. J.* 80 (11), 1023. doi:10.1140/epjc/s10052-020-08616-1
- Ponglertsakul, S., Burikham, P., and Tannukij, L. (2018). Quasinormal modes of black strings in de Rham-Gabadadze-Tolley massive gravity. *Eur. Phys. J. C* 78 (7), 584. doi:10.1140/epjc/s10052-018-6057-9
- Quevedo, H. (2008). Geometrothermodynamics of black holes. *Gen. Rel. Grav.* 40, 971–984. doi:10.1007/s10714-007-0586-0
- Quevedo, H., and Sanchez, A. (2008). Geometrothermodynamics of asymptotically de Sitter black holes. *JHEP*, 09:034. doi:10.1088/1126-6708/2008/09/034

- Rezzolla, L., and Zhidenko, A. (2014). New parametrization for spherically symmetric black holes in metric theories of gravity. *Phys. Rev. D.* 90 (8), 084009. doi:10.1103/physrevd.90.084009
- Robert, C. (2010). Myers and brandon robinson. black holes in quasi-topological gravity. *JHEP* 08, 067. doi:10.1007/JHEP08(2010)067
- Sajadi, S. N., and Hendi, S. H. (2022). Analytically approximation solution to einstein-cubic gravity. *Eur. Phys. J.* 82 (8), 675. doi:10.1140/epjc/s10052-022-10647-9
- Sajadi, S. N., Mann, R. B., Riazi, N., and Fakhry, S. (2020). Analytically approximation solution to higher derivative gravity. 10. doi:10.1103/PhysRevD.102.124026
- Sajadi, S. N., Shahkarami, L., Charmchi, F., and Hendi, S. H. (2022). Charged black holes in Einsteinian quartic gravity. *Ann. Phys.* 447, 169162. doi:10.1016/j.aop.2022.169162
- Sajadi, S. N., Mann, R. B., Sheikahmadi, H., and Khademi, M. (2024). Black hole solutions to einstein-bel-robinson gravity. *JHEP* 11, 041. doi:10.1007/jhep11(2024)041
- Salvio, A. (2018). Quadratic gravity. *Front. Phys.* 6, 77. doi:10.3389/fphy.2018.00077
- Senjaya, D., and Ponglertsakul, S. (2025). The extreme Reissner–Nordström black hole: new exact solutions to the Klein–Gordon equation with minimal coupling. *Ann. Phys.* 473, 169898. doi:10.1016/j.aop.2024.169898
- Stelle, K. S. (1977). Renormalization of higher derivative quantum gravity. *Phys. Rev. D.* 16, 953–969. doi:10.1103/physrevd.16.953
- Thomas, P. (2010). Sotiriou and valerio Faraoni. f(R) theories of gravity. *Rev. Mod. Phys.* 82, 451–497. doi:10.1103/RevModPhys.82.451
- Wald, R. M. (1993). Black hole entropy is the Noether charge. *Phys. Rev. D.* 48 (8), R3427–R3431. doi:10.1103/physrevd.48.r3427
- Xiao, Y., Liu, Y.-X., Tian, Yu, and Zhang, H. (2025). *Explicit Universal Formula Thermodynamic Volume Extended Black Hole Thermodynamics* 12.
- Zimmerman, A., and Mark, Z. (2016). Damped and zero-damped quasinormal modes of charged, nearly extremal black holes. *Phys. Rev. D.* 93 (4), 044033. doi:10.1103/physrevd.93.044033
- Zinhailo, A. F. (2018). Quasinormal modes of the four-dimensional black hole in Einstein–Weyl gravity. *Eur. Phys. J.* 78 (12), 992. doi:10.1140/epjc/s10052-018-6467-8

Appendix A: Near-horizon constants

Here, we present the near-horizon constants f_4 and f_5 as follows.

$$f_4 = -\frac{1}{96r_+^4 \mathcal{K} f_1^2 (r_+ f_1 + 2)} (312\mathcal{K}r_+^4 f_1^2 f_2 f_3 + 96\mathcal{K}r_+^4 f_1 f_2^2 - 220\mathcal{K}r_+^2 f_1^2 f_3 - 312\mathcal{K}r_+^2 f_1 f_2^2 + 336\mathcal{K}r_+^3 f_1 f_2 f_3 + 32\mathcal{K}r_+^3 f_2^2 + 296\mathcal{K}r_+^2 f_1^2 f_2 + 12r_+^6 f_3 - 312\mathcal{K}r_+^2 f_1^2 f_3 - 228\mathcal{K}r_+^2 f_1 f_2^2 - 81\mathcal{K}r_+ f_1^4 + 4\Lambda r_+^5 + 12r_+^5 f_2 + 360\mathcal{K}r_+ f_1^2 f_2 - 112\mathcal{K}f_1^3 + 12q^2 r_+), \quad (60)$$

$$f_5 = -\frac{1}{180r_+^4 \mathcal{K} f_1^2 (r_+ f_1 + 2)} (648\mathcal{K}r_+^5 f_1^2 f_2 f_4 + 342\mathcal{K}r_+^5 f_1^2 f_3 + 672\mathcal{K}r_+^5 f_1 f_2 f_3 + 48\mathcal{K}r_+^5 f_4^2 - 436\mathcal{K}r_+^4 f_1^3 f_4 - 1332\mathcal{K}r_+^4 f_1^2 f_2 f_3 - 416\mathcal{K}r_+^4 f_1 f_2^2 + 720\mathcal{K}r_+^4 f_1 f_2 f_4 + 360\mathcal{K}r_+^4 f_1 f_3^2 + 240\mathcal{K}r_+^4 f_2^2 f_3 + 596\mathcal{K}r_+^3 f_1^2 f_3 + 888\mathcal{K}r_+^3 f_1 f_2^2 + 12r_+^7 f_4 - 600\mathcal{K}r_+^3 f_1^2 f_4 - 1200\mathcal{K}r_+^3 f_1 f_2 f_3 - 160\mathcal{K}r_+^3 f_2^2 - 660\mathcal{K}r_+^2 f_1^2 f_2 + 12r_+^6 f_3 + 720\mathcal{K}r_+^2 f_1^2 f_3 + 720\mathcal{K}r_+^2 f_1 f_2^2 + 157\mathcal{K}r_+ f_1^4 - 720\mathcal{K}r_+ f_1^2 f_2 + 200\mathcal{K}f_1^3 - 12q^2 r_+). \quad (61)$$

Appendix B: Explicit terms in the continued fraction approximation

We present terms up to the fourth order in the continued fraction approximation:

$$\begin{aligned} \epsilon &= -\frac{F_1}{r_+} - 1, \quad a_1 = -1 - a_0 + 2\epsilon + r_+ f_1, \quad a_2 = -\frac{4a_1 - 5\epsilon + 1 + 3a_0 + f_2 r_+^2}{a_1}, \\ a_3 &= -\frac{1}{a_1 a_2} [-f_3 r_+^3 + a_1 a_2^2 + 5a_1 a_2 + 6a_0 + 10a_1 - 9\epsilon + 1], \\ a_4 &= -\frac{f_4 r_+^4 + a_1 a_2^3 + 2a_1 a_2^2 a_3 + a_1 a_2 a_3^2 + 6a_1 a_2^2 + 6a_1 a_2 a_3 + 15a_1 a_2 + 10a_0 + 20a_1 - 14\epsilon + 1}{a_1 a_2 a_3}. \end{aligned} \quad (62)$$

Appendix C: Chemical potentials

The action of Maxwell theory is given by

$$I_{EM} = -\frac{1}{16\pi} \int d^4x \sqrt{-g} F_{\mu\nu} F^{\mu\nu}, \quad (63)$$

Here, $F = dA$, $A = A_t(r)dt$, and the Maxwell equation is $\nabla_\mu F^{\mu\nu} = 0$. For a static spherical symmetric, we have

$$F_{tr} = \frac{q}{r^2}, \quad \rightarrow \quad A_t(r) = -\frac{q}{r} + C. \quad (64)$$

The constant C should be determined by regularity. From the regularity of the gauge potential on the horizon, we have $A_\mu \xi^\mu|_{r_+} = 0$ for $\xi = \partial_t$. From here, we obtain C as follows:

$$C = \frac{q}{r_+}, \quad \rightarrow \quad A_t(r) = \frac{q}{r_+} - \frac{q}{r}. \quad (65)$$

Using the Iyer–Wald approach ($\delta H_\infty = \psi_q \delta q$) (Wald, 1993; Iyer and Wald, 1994), the electric contribution at infinity is

$$\psi_q = \frac{q}{r_+}. \quad (66)$$

This is the thermodynamic electric potential. Similarly, in the following, we obtain the chemical potentials for the coupling constant and cosmological constant. Here, the coupling constant $\tilde{\alpha}_i$ is promoted to the scalar function $\tilde{\alpha}_i(x)$. The field strength $F_{\tilde{\alpha}_i}(x)$ is implemented in the following Lagrangian:

$$L = \frac{1}{16\pi} \left(R - 2\Lambda(x)(1 - F_\Lambda(x)) - \sum_{i=1}^6 \tilde{\alpha}_i(x) (\tilde{\mathcal{L}}^i - F_{\tilde{\alpha}_i}(x)) \right) \epsilon. \quad (67)$$

By variation of the Lagrangian with respect to the field $\tilde{\alpha}_i$ and $\Lambda(x)$, equations of motion are derived, which imply the following on-shell relations:

$$F_{\tilde{\alpha}_i}(x) = \tilde{\mathcal{L}}^i \epsilon = \sqrt{-g} \tilde{\mathcal{L}}^i dt \wedge dr \wedge d\theta \wedge d\phi, \quad (68)$$

$$F_\Lambda(x) = \epsilon = \sqrt{-g} dt \wedge dr \wedge d\theta \wedge d\phi. \quad (69)$$

Therefore, the field strength can be written explicitly as

$$F_{\mathcal{K}}(x) = -\frac{\sin(\theta) f'^2}{24\pi r^3} \left(2(f-1)f' - \frac{5r}{4} f'^2 + r f'' (r f' + 3 - 3f) \right) dt \wedge dr \wedge d\theta \wedge d\phi, \quad (70)$$

$$F_\Lambda(x) = -\frac{r^2 \sin(\theta)}{8\pi} dt \wedge dr \wedge d\theta \wedge d\phi, \quad (71)$$

where \mathcal{K} is defined in Equation 5. The gauge fields are

$$A_{\mathcal{K}}(x) = -\left[\frac{f'^3 (f' r + 4 - 4f)}{80\pi r^2} + Y \right] \sin \theta dt \wedge d\theta \wedge d\phi, \quad (72)$$

$$A_\Lambda(x) = -\frac{\sin(\theta)}{8\pi} \left[\frac{r^3}{3} + Y' \right] dt \wedge d\theta \wedge d\phi. \quad (73)$$

Therefore, the corresponding chemical potentials are given as

$$\psi_{\mathcal{K}} = -\left[\frac{f_1^3 (r_+ f_1 + 4)}{24r_+^2} + Y \right], \quad (74)$$

$$\psi_\Lambda = -\left[\frac{r_+^3}{6} + Y' \right]. \quad (75)$$

The second terms in the parentheses are pure gauges, which should be determined by background subtraction.

Appendix D: A brief review of Mashhoon's method

According to this method, the QNMs of a potential barrier are related to the bound states of the inverted potential. Let p be a set of parameters associated with the potential. These may already belong to the potential or be introduced as scaling parameters. The parameterized potential is denoted by $U(x;p)$; the wave functions and the quasi-normal frequencies are also functions of the parameters p : $\psi = \psi(x;p)$ and $w = w(p)$. Now, we introduce the formal transformations $x \rightarrow -ix$ and $p \rightarrow p' = \Pi(p)$ in such a way that the potential remains invariant:

$$U(-ix;p') = U(x;p), \quad (76)$$

Here, x is the tortoise coordinate. Let us define ϕ and Ω such that $\phi(x;p) = \psi(-ix;p')$ and $\Omega(p) = w(p')$.

Then, ϕ satisfies the Schrödinger-like equation:

$$\frac{d^2 \phi}{dx^2} + (-\Omega^2 + U) \phi = 0. \quad (78)$$

The boundary conditions corresponding to the QNMs are

$$\phi(x;p) \propto \exp(\mp \Omega x) \quad \text{as} \quad x \rightarrow \pm \infty. \quad (79)$$

Once $\Omega(p)$ is determined, the quasi-normal frequencies are found by the inverse transformation:

$$w(p) = \Omega(\Pi^{-1}(p)) \quad \text{and} \quad \psi(x;p) = \phi(ix;\Pi^{-1}(p)). \quad (80)$$

The QNMs that are directly related, through (80), to the true bound states of the inverted potential will be referred to as proper QNMs. For instance, let us consider the potential $U(x)$, which decreases exponentially to 0 at $x \rightarrow -\infty$ but falls off as x^{-2} for $x \rightarrow +\infty$. In this case, one can estimate $U(x)$ by using a simpler potential that only matches the original potential near its maximum. This simple potential is the Poschl–Teller potential:

$$U_{PT} = \frac{U_0}{\cosh^2 \alpha (x - x_0)}. \quad (81)$$

The quantities U_0 and $\alpha > 0$ are given by the height and curvature of the potential at its maximum ($x = x_0$). These are

$$U_0 = U(x_0), \quad \alpha^2 = -\frac{1}{2U_0} \left. \frac{d^2 U}{dx^2} \right|_{x_0}. \quad (82)$$

The transition from the potential barrier U_{PT} to the inverted potential is achieved by the transformations $x \rightarrow -ix$ (U_0, α) and

$\rightarrow (U_0, i\alpha)$. The bound states of $-U_{PT}$ are given by

$$\Omega_n(U_0, \alpha) = \alpha \left[-\left(n + \frac{1}{2}\right) + \left(\frac{1}{4} + \frac{U_0}{\alpha^2}\right)^{\frac{1}{2}} \right]. \quad (83)$$

The proper QNMs may be obtained from $\Omega_n(U_0, -i\alpha)$, and the corresponding frequencies are given by

$$w_r = \pm \left(U_0 - \frac{\alpha^2}{4}\right)^{1/2}, \quad w_i = \alpha \left(n + \frac{1}{2}\right). \quad (84)$$

Therefore, roughly speaking, the height of the potential barrier is the characteristic real part of QNM ($\omega_r \approx \sqrt{U_0}$). Therefore, higher barriers lead to larger oscillation frequencies. The curvature at the maximum of the effective potential controls the damping rate of perturbations ($\omega_i \approx U_0'$). Therefore, the sharper/broader peak of the effective potential corresponds to fast-damping/long-lived modes (Kokkotas and Schmidt, 1999; Berti et al., 2009).